

STABILITY, RELAXATION, AND OSCILLATION OF BIODEGRADATION FRONTS*

JACK X. XIN[†] AND JAMES M. HYMAN[‡]

Abstract. We study the stability and oscillation of traveling fronts in a three-component, advection-reaction biodegradation model. The three components are pollutant, nutrient, and bacteria concentrations. Under an explicit condition on the biomass growth and decay coefficients, we derive reduced, two-component, semilinear hyperbolic models through a relaxation procedure, during which biomass is slaved to pollutant and nutrient concentration variables. The reduced two-component models resemble the Broadwell model of the discrete velocity gas. The traveling fronts of the reduced system are explicit and are expressed in terms of hyperbolic tangent function in the nutrient-deficient regime. We perform energy estimates to prove the asymptotic stability of these fronts under explicit conditions on the coefficients in the system. In the small damping limit, we carry out Wentzel–Kramers–Brillouin (WKB) analysis on front perturbations and show that fronts are always stable in the two-component models. We extend the WKB analysis to derive amplitude equations for front perturbations in the original three-component model. Because of the bacteria kinetics, we find two asymptotic regimes where perturbation amplitudes grow or oscillate in time. We perform numerical simulations to illustrate the predictions of the WKB theory.

Key words. biodegradation, fronts, stability, growth, oscillation

AMS subject classifications. 35L60, 35R35, 41A60, 65D30

PII. S003613999732696X

1. Introduction. Bioremediation is a promising biological method for restoring groundwater and soil contaminated with organic pollutants because of the advantages of low cost and in situ flexibility. A remedial procedure typically involves the injection of a limiting nutrient (O_2 , or electron acceptor) into aquifers with pollutants serving as the substrate (electron donor), in order to generate a biologically active zone (BAZ), where significant amounts of the indigenous bacteria grow to consume the pollutants.

Bioremediation was first systematically studied in theory and field applications in [1], [2], then modeled numerically in [14], [13], [6], [8] among others. See [17] for the discussions of bioremediation from the technological and practical viewpoints. The above works showed that bioremediation is a complicated physical-chemical-biological process involving groundwater flow (advection/diffusion), microbial growth (nonlinear reaction), and heterogeneity (spatial variability). To extract key features of dynamics, coherent structures are particularly helpful. More recently, the role of traveling fronts in understanding the pollutant removal rates have been observed and analyzed in [19], [16]. See also [7], [23] for studies of traveling fronts in spatially random porous media; [20], [22] for variable speed spherical fronts in two and three space dimensions.

One of the basic mathematical models characterizing the essentials of a biodegradation process was proposed and studied in Odencrantz, Valocchi, and Rittmann [18],

*Received by the editors September 10, 1997; accepted for publication (in revised form) March 4, 1999; published electronically August 3, 2000.

<http://www.siam.org/journals/siap/61-2/32696.html>

[†]Department of Mathematics, Texas Institute of Computational and Applied Mathematics, University of Texas, Austin, TX 78712 (jxin@math.utexas.edu). The research of this author was partially supported by National Science Foundation grant DMS-9625680. The computations were carried out at both the University of Arizona and Los Alamos National Laboratory.

[‡]Group T-7, MS B284, Los Alamos National Laboratory, Los Alamos, NM 87545 (in@lanl.gov). The research of this author was supported by the Department of Energy Applied Mathematics Sciences contract KC-07-01-01.

and in Oya and Valocchi [19]:

$$(1.1) \quad R_f S_t = DS_{xx} - vS_x - \frac{MAS}{(K_A + A)(K_S + S)},$$

$$(1.2) \quad A_t = DA_{xx} - vA_x - \gamma \frac{MAS}{(K_A + A)(K_S + S)},$$

$$(1.3) \quad M_t = -b(M - M_b) + Y \frac{MAS}{(K_A + A)(K_S + S)},$$

where

S : the pollutant (substrate) concentration;

A : the nutrient concentration;

M : the bacteria population or biomass;

$R_f > 1$: the substrate retardation factor;

$D \geq 0$: hydrodynamic diffusion constant;

$v > 0$: pore water velocity;

K_A and $K_S > 0$: half-saturation constants of nutrient A and substrate S ;

b and $Y > 0$: decay and yield constants of biomass M ;

$M_b > 0$: natural biomass population;

$\gamma > 0$: stoichiometric constant for nutrient consumption by substrate.

The product form of nonlinearity in (1.1)–(1.3) is the commonly used Monod kinetic. In [19] there is a constant q_m , the maximum substrate utilization rate, multiplying the Monod nonlinear terms. This constant is normalized to one in (1.1)–(1.3).

We analyze the situation in which the nutrient is injected from the left end of a uniform tube where initial biomass and pollutants reside. The entering nutrient advects at a higher velocity v than that of the pollutant, $R_f^{-1}v$. Hence, mixing occurs between these two over a certain spatial domain and causes the bacteria to grow. The growth of bacteria consumes both the nutrient and pollutants, and eventually the three components move together to the right. Mathematically, it is convenient to formulate the problem on the whole line, and the above process can then be described by the motion of traveling fronts. We are thus led to consider the initial value problem for (1.1)–(1.3) with bounded, nonnegative, measurable initial data. Moreover, $(S, A, M)(0, x) \rightarrow (S_+, 0, M_b)$ as $x \rightarrow +\infty$, and $(S, A, M)(0, x) \rightarrow (0, A_-, M_b)$ as $x \rightarrow -\infty$, where S_+, A_- are positive constants, representing the input of nutrient concentration A_- from the left into a medium with pollutant concentration S_+ and biomass M_b .

Murray and Xin [16] proved that if $R_f > 1$ and $D \geq 0$, system (1.1)–(1.3) always admits a constant-speed, traveling-wave solution $(S(x - c_0t), A(x - c_0t), M(x - c_0t), c_0)$ satisfying the boundary conditions

$$(1.4) \quad S(-\infty) = 0, \quad S(+\infty) = S_+, \quad A(-\infty) = A_-, \quad A(+\infty) = 0, \quad M(\pm\infty) = M_b.$$

Defining $\xi = x - c_0t$, the traveling wave satisfies

$$(1.5) \quad 0 < S(\xi) < S_+, \quad S'(\xi) > 0, \quad 0 < A(\xi) < A_-, \quad A'(\xi) < 0 \quad \forall \xi,$$

$$(1.6) \quad c_0 = \frac{v(A_- + \gamma S_+)}{A_- + \gamma R_f S_+},$$

$$(1.7) \quad M_b < M \leq M_b + Y \frac{(R_f - 1)A_- S_+}{A_- + \gamma S_+} \quad \forall \xi \in R^1.$$

We see that S is strictly monotone increasing and A is strictly monotone decreasing in ξ . Moreover, the estimates (1.5)–(1.6) are independent of D . It is shown in [16] that the viscous ($D > 0$) traveling waves converge to a limiting inviscid smooth traveling wave as $D \rightarrow 0$, satisfying the same bounds (1.5)–(1.7). As we discuss in detail in a later section, these inviscid traveling waves can be obtained much more easily by a phase plane analysis and they are unique up to a constant translation in ξ . The positive D does not change the traveling front speeds (1.6). A small positive D only slightly enlarges the width of fronts and has little effect on the dynamics because the system is predominantly advection-reaction. The same observation goes for the small amount of numerical diffusion in our simulations. *Hence in the rest of this paper, we shall consider only the $D = 0$ limit of the system (1.1)–(1.3).*

The existence of constant speed fronts does not mean, however, that they are dynamically attracting. In general, front solutions can move at constant speeds or time-dependent speeds (oscillatory), depending on the parameter regimes (see [19]). It is this interesting dynamical issue that we address in this paper. The inviscid regime $D = 0$ is the convenient one for carrying out the analysis, in terms of either simple forms of traveling fronts or the front stability and oscillation.

We develop two key elements of the approach. The first is the observation that the A and S equations can be expressed as a conservative form in the new variables $u = \gamma R_f S - A$, $w = \gamma S - A$. One sees at once that there is a conserved quantity of the system, namely, the integral $\int u = \int \gamma R_f S - A$. As a direct consequence, the speed of the traveling front is explicitly given by a Rankine–Hugoniot relation (see (1.6) of this paper) [11]. The second element is to derive simplified two-component and scalar models in the relaxation (large space and time) limit of the original system in conservative form. The two-component models have more explicit front solutions and help us gain understanding. In the nutrient-deficient (ND) regime (K_A and K_S are much larger than S_+ , A_-) of the two-equation model, we make use of the conserved quantity $\int u$ to write the two equations of (A, S) into a single damped-driven wave equation with two distinct characteristic speeds, as long as the initial perturbation has zero spatial integral. It is this further reduction and the resulting wave equation that allows us to perform energy estimates and Wentzel–Kramers–Brillouin (WKB) analysis on front perturbations. The WKB analysis then extends to the original system to reveal front oscillations that are due to biomass kinetics. The analytical findings so obtained agree qualitatively with our direct finite-difference numerical simulations.

Even the reduced two-component system has rich dynamical properties. In the ND regime or when K_A and K_S are not small, we observe traveling-front stability. In the extreme ND regime (K_A and K_S tend to zero), we recover the two-equation model studied in [19], where explicit oscillatory fronts are constructed. It is unknown whether these oscillatory fronts persist or eventually damped for any positive K_A and K_S , which requires a more refined analysis to address.

The rest of the paper is organized as follows. In section 2 we derive two-component models in the relaxation limit. There are two interesting regimes, the ND regime, where fronts are stable, and the nutrient-sufficient regime, where fronts are oscillatory. In section 3 we discuss explicit constant-speed traveling fronts in the ND regime of the two-component model, as well as those in closed form in the more general two-component model (where K_A and K_S stay away from zero). We also illustrate the traveling front of the original three-component model (with $D = 0$) as a saddle-node connection on the phase plane. In section 4 we carry out the asymptotic stability analysis on the traveling fronts in the ND, two-component model. In section 5 we perform

WKB analysis in the small damping limit (or $M_b R_f^{-1} (R_f - 1)^{-1} (K_A K_S)^{-1} \ll 1$). In the two-component model, we derive amplitude equations for small front perturbations and find that front damping always exists. There is more damping to the faster (slower) moving perturbation to the right (left) of the front than to the left (right). In the ND regime of the original three-component model, we identify the source of front instability by deriving amplitude equations which show that perturbations can grow and oscillate in time in two regimes of parameters. One regime is oscillatory and occurs when both the retardation factor R_f is large and $K_A = K_S = R_f^{-\alpha}$ is small, where $\alpha \in [\frac{1}{2}, 1)$. The other regime shows front growth for transient time and occurs when $Y, K_A = K_S$ are large and R_f is close to one. In section 6 we show numerical results of second- and higher-order finite difference methods on the two- and three-component models. The analytical predictions in sections 4 and 5 agree qualitatively with the numerics. Comparison of the two-equation models with the full three-equation model show that the two-equation models approximate well in terms of the front speed and profiles if the relaxation condition (2.17) holds. Section 7 is the appendix for energy estimates, and section 8 contains a summary of results in the paper.

2. Derivation of two-component models.

2.1. Conservative form of the system. Hereafter, we consider the inviscid ($D = 0$) three-component biodegradation system:

$$(2.1) \quad R_f S_t + v S_x = - \frac{MAS}{(K_A + A)(K_S + S)},$$

$$(2.2) \quad A_t + v A_x = -\gamma \frac{MAS}{(K_A + A)(K_S + S)},$$

$$(2.3) \quad M_t = -b(M - M_b) + Y \frac{MAS}{(K_A + A)(K_S + S)}.$$

The change of variables,

$$(2.4) \quad u = \gamma R_f S - A, \quad w = \gamma S - A,$$

or

$$(2.5) \quad A = A(u, w) = (R_f - 1)^{-1}(u - R_f w), \quad S = S(u, w) = \gamma^{-1}(R_f - 1)^{-1}(u - w),$$

transforms (2.1)–(2.3) into the conservative form

$$(2.6) \quad u_t + v w_x = 0,$$

$$(2.7) \quad w_t + v((1 + R_f^{-1})w - R_f^{-1}u)_x = \tilde{\epsilon}(u - w)(u - R_f w)M/G,$$

$$(2.8) \quad M_t = -b(M - M_b) + Y \frac{MAS}{(K_A + A)(K_S + S)},$$

where

$$\tilde{\epsilon} = R_f^{-1}(R_f - 1)^{-1}(K_A K_S)^{-1},$$

$A = A(u, w), S = S(u, w)$, and $G = G(A(u, w), S(u, w))$, with

$$(2.9) \quad G(A, S) = (1 + K_A^{-1}A)(1 + K_S^{-1}S) > 0.$$

The integral $\int u$ is conserved as (2.6) shows. System (2.6)–(2.8) is reminiscent of the Broadwell model

$$(2.10) \quad \rho_t + m_x = 0,$$

$$(2.11) \quad m_t + z_x = 0,$$

$$(2.12) \quad z_t + v^2 m_x = \{(v^2 \rho - z)^2 - 4(z^2 - v^2 m^2)\}/8v^2.$$

For discrete velocity gas motion, where $v > 0$ is given, see [3]. A well-known property [4], [24] of (2.10)–(2.12) is that in the large space and time limit, the solutions converge to those of the reduced system (2.10)–(2.11) with the variable z given by (ρ, m) setting the right side of (2.12) to zero. The limit is also known as the fluid dynamic limit or relaxation [5], [9], similar to the derivation of Euler or Navier–Stokes equations from the Boltzmann equation in kinetic theory.

2.2. Relaxation and two-component models. Let us examine (2.6)–(2.8) under the hyperbolic scaling $x \rightarrow \frac{x}{\epsilon}$, $t \rightarrow \frac{t}{\epsilon}$, $\epsilon \rightarrow 0^+$, suitable for studying the behavior of frontlike solutions. The scaled system reads

$$(2.13) \quad u_t + vw_x = 0,$$

$$(2.14) \quad w_t + v((1 + R_f^{-1})w - R_f^{-1}u)_x = \epsilon^{-1}\tilde{\epsilon}(u - w)(u - R_f w)M/G,$$

$$(2.15) \quad M_t = \epsilon^{-1} \left(-b(M - M_b) + Y \frac{MAS}{(K_A + A)(K_S + S)} \right).$$

The right side of (2.15) relaxes to its equilibrium state, or

$$(2.16) \quad -b(M - M_b) + Y \frac{MAS}{(K_A + A)(K_S + S)} = 0,$$

to the leading order, provided the partial derivative of the left side to M is negative (stability requirement for relaxation [5]). This is the case if

$$(2.17) \quad \frac{YA_-S_+}{(K_A + A_-)(K_S + S_+)} < b.$$

Solving (2.16) gives

$$(2.18) \quad M = bM_b \left(b - \frac{YAS}{(K_A + A)(K_S + S)} \right)^{-1}.$$

Similarly, the right side of (2.14) also relaxes to its equilibrium state, or

$$(2.19) \quad (u - w)(u - R_f w) = 0,$$

which has two solutions, either $w = u$ or $w = R_f^{-1}u$. By relaxation stability, the partial derivative

$$[(u - w)(u - R_f w)M/G]_w$$

should be negative at $w = u$ or at $w = R_f^{-1}u$. This means that

$$[(u - w)(u - R_f w)]_w = 2R_f w - (1 + R_f)u$$

must be negative at either equilibrium. At $w = u$, this derivative is equal to $(R_f - 1)u$; at $w = R_f^{-1}u$, it is equal to $(1 - R_f)u$. Therefore, $w = u$ ($w = R_f^{-1}u$) only if $u < 0$ ($u > 0$), which implies that

$$(2.20) \quad w = f(u) \equiv u(1 - H(u)) + R_f^{-1}uH(u),$$

where the Heaviside function $H(u) = 1$, if $u > 0$; otherwise, $H(u) = 0$. The final relaxed equation is

$$(2.21) \quad u_t + (f(u))_x = 0,$$

with two other components given by (2.20) and (2.18). The rigorous justification of this limiting process is discussed in [15], where strong convergence of solutions as $\epsilon \rightarrow 0$ in space and time L^1 corresponds to the stable front regime. Equation (2.21) is a scalar conservation law with piecewise linear and convex flux function.

We now propose a two-component model taking into account the M relaxation (2.18) but keeping the (u, w) or (A, S) equations the same. Though simpler than the original system, this model preserves more structures than a scalar equation in that traveling waves are still smooth functions and not shock waves. Moreover, the two-component model and the original system share the same relaxation limit. A special two-component model is studied in [19] for oscillatory fronts.

We proceed with the derivation by updating the reaction term in (2.1)–(2.2) with (2.18):

$$(2.22) \quad R = \frac{M_b AS}{K_A K_S + K_A S + K_S A + (1 - b^{-1}Y)AS}.$$

The reduced system becomes

$$(2.23) \quad R_f S_t = -v S_x - \epsilon^{-1} R,$$

$$(2.24) \quad A_t = -v A_x - \epsilon^{-1} \gamma R.$$

We undo the scaling in (2.23)–(2.24) to recover the two-equation system:

$$(2.25) \quad R_f S_t = -v S_x - R,$$

$$(2.26) \quad A_t = -v A_x - \gamma R,$$

with R given by (2.22). We call (2.25)–(2.26) the general two-component model.

A solution of the two-component model is expected to be only close to that of the original system when time is large. For early and intermediate times, they are in general different unless the decay and yield coefficients (b, Y) are large while satisfying (2.17).

2.3. Nutrient-deficient model. There are *two distinguished limits* in the general two-component model. The first limit occurs when $(K_A, K_S) \gg O((A_-, S_+))$, the ND regime; the second limit occurs when $(K_A, K_S) \ll O((A_-, S_+))$, the nutrient-sufficient regime.

In the first limit, we can further simplify (2.23)–(2.24):

$$(2.27) \quad R_f S_t + v S_x = -\frac{M_b}{K_A K_S} AS,$$

$$(2.28) \quad A_t + v A_x = -\frac{\gamma M_b}{K_A K_S} AS,$$

which will be called the ND model.

In the second limit, R tends to $M_{ns} \equiv M_b(1 - b^{-1}Y)^{-1}$ times the Heaviside function $H(AS)$ ($H = 1$ if $AS > 0$, $H = 0$ if $AS = 0$). The system becomes

$$(2.29) \quad R_f S_t = -v S_x - M_{ns} H(AS),$$

$$(2.30) \quad A_t = -v A_x - \gamma M_{ns} H(AS),$$

which has been integrated explicitly in [19] to find oscillatory traveling-front solutions of the form $(S, A) = (S, A)(x - ct, t)$, periodic in t . The period of front temporal oscillation T is

$$(2.31) \quad T = \frac{A_-}{\gamma M_{ns}} \left(\frac{S_+ \gamma R_f}{A_-} + 1 \right),$$

implying that $T = O(R_f)$ for large R_f .

Using both rigorous and formal analysis, we show that in the ND model the constant-speed traveling fronts (available in closed form) are dynamically stable. The formal asymptotic analysis also extends to the original three-component model to provide information on front oscillations.

3. Inviscid traveling fronts.

3.1. Explicit fronts in two-component models. Explicit traveling-front solutions of the form $(u_0, w_0)(\xi)$, $\xi = x - ct$, exist in the ND, two-component model (that is, (2.6)–(2.7) with $M = M_b$ and $G = 1$):

$$(3.1) \quad u_t + v w_x = 0,$$

$$(3.2) \quad w_t + v((1 + R_f^{-1})w - R_f^{-1}u)_x = \tilde{\epsilon}(u - w)(u - R_f w)M_b.$$

The formulas are

$$(3.3) \quad c_0 = v \frac{\gamma S_+ + A_-}{\gamma R_f S_+ + A_-},$$

$$(3.4) \quad u_0 = \frac{v}{c_0} w_0 + \left(-1 + \frac{v}{c_0}\right) A_-,$$

$$(3.5) \quad w_0 = \frac{\gamma S_+ - A_-}{2} + \frac{\gamma S_+ + A_-}{2} \tanh\left(\frac{1}{2v} R_f (\gamma R_f S_+ + A_-) \tilde{\gamma} \xi\right),$$

where $\tilde{\gamma} = M_b \tilde{\epsilon}$. Such solutions are unique up to a constant translation in ξ . In the original variables (S, A) we have, in view of (2.5) and (3.3), the *explicit expression of traveling fronts* of system (2.27)–(2.28):

$$(3.6) \quad A(\xi) = \frac{A_-}{2} \left(1 - \tanh\left(\frac{M_b}{K_A K_S} \frac{A_- + \gamma R_f S_+}{2(R_f - 1)} \xi\right) \right)$$

and

$$(3.7) \quad S(\xi) = \frac{S_+}{2} \left(1 + \tanh\left(\frac{M_b}{K_A K_S} \frac{A_- + \gamma R_f S_+}{2(R_f - 1)} \xi\right) \right),$$

where c_0 is given in (3.3). To derive the formulas (3.3)–(3.5), we substitute the form of traveling fronts in (2.6)–(2.7) to get

$$(3.8) \quad -c_0 u'_0 + v w'_0 = 0,$$

$$(3.9) \quad -c_0 w'_0 + v(-R_f^{-1} u'_0 + (1 + R_f^{-1}) w'_0) = \tilde{\gamma}(u_0 - w_0)(u_0 - R_f w_0).$$

Integrating (3.8) in ξ and applying the boundary conditions at infinity yield (3.3) and (3.4). Plugging (3.4) into (3.9), we get

$$\begin{aligned} & -c_0 w'_0 + v(1 + R_f^{-1}) w'_0 - \frac{v}{R_f} c_0^{-1} v w'_0 \\ &= \tilde{\gamma} \left(\left(\frac{v_0}{c_0} - 1 \right) w_0 + \left(\frac{v - c_0}{c_0} \right) A_- \right) \left(\left(\frac{v_0}{c_0} - R_f \right) w_0 + \left(\frac{v - c_0}{c_0} \right) A_- \right) \end{aligned}$$

or

$$\begin{aligned} & \left(-c_0 + v(1 + R_f^{-1}) - \frac{v^2}{R_f} c_0^{-1} \right) w'_0 \\ &= \tilde{\gamma} \left(\frac{v_0}{c_0} - 1 \right) \left(\frac{v_0}{c_0} - R_f \right) (w_0 + A_-) \left(w_0 + \frac{v - c_0}{v - R_f c_0} A_- \right). \end{aligned}$$

Using (3.3), the above equality becomes

$$(3.10) \quad w'_0 = - \frac{\tilde{\gamma} R_f (\gamma R_f S_+ + A_-)}{v(\gamma S_+ + A_-)} (w_0 + A_-)(w_0 - \gamma S_+).$$

Recall that the ordinary differential equation (ODE) ($\alpha > 0, a_1 < a_2$),

$$w' = -\alpha(w - a_1)(w - a_2),$$

under the boundary conditions $w(-\infty) = a_1, w(+\infty) = a_2$, has a unique solution:

$$w = \frac{1}{2}(a_1 - a_2) \tanh \left(\frac{\alpha}{2}(a_1 - a_2)\xi \right) + \frac{a_1 + a_2}{2},$$

up to a constant translation in ξ . The formula (3.5) follows. We see from (3.4) and (3.5) that the wave profiles are strictly increasing in ξ :

$$(3.11) \quad u'_0 > 0, \quad w'_0 > 0 \quad \forall \xi.$$

In view of (2.4), (2.5), and (3.4), we have from (3.11)

$$(3.12) \quad A'_0 < 0, \quad S'_0 > 0 \quad \forall \xi.$$

The general two-component model system (2.25)–(2.26), (2.22) also has the traveling fronts in closed form. In fact, it is easy to verify that (3.3)–(3.4) remains the same and that (3.10) is replaced by

$$(3.13) \quad w'_0 = - \frac{\tilde{\gamma} R_f (\gamma R_f S_+ + A_-)}{v(\gamma S_+ + A_-)} (w_0 - \gamma S_+)(w_0 + A_-)/G(w_0),$$

where $G(w_0) = F(A(w_0), S(w_0))$, where $A = A(w_0)$ and $S = S(w_0)$ are A and S expressed as functions of w_0 using (2.5) and (3.4), and where $F = F(A, S)$ is

$$(3.14) \quad F(A, S) = 1 + S/K_S + A/K_A + (1 - b^{-1}Y)AS/(K_A K_S).$$

Equation (3.13) can be integrated, and w_0 expressed in terms of the inverse of logarithmic functions. Details are carried out in Xin and Zhang [23], where random porosity effects on front structures are analyzed for the two-component models.

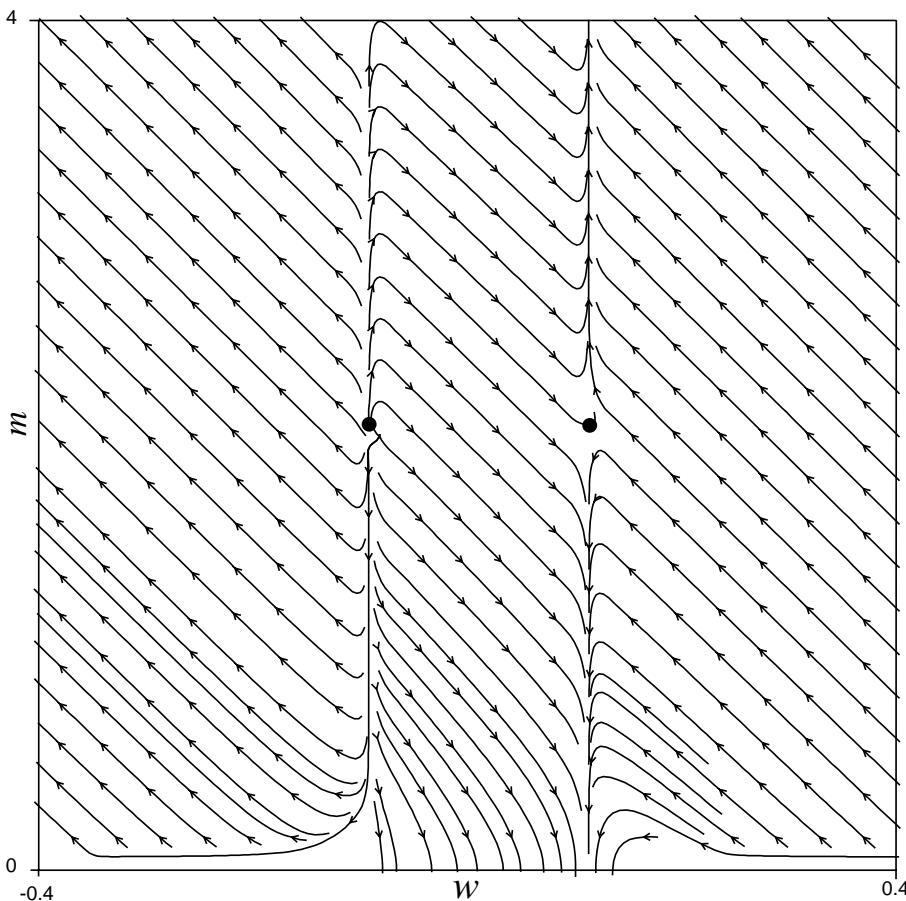


FIG. 1. Phase portrait of the system (3.20) on the (w, m) plane. The upper half of the phase plane $m \geq 2$ is meaningful for this model and the unique connection from the unstable node $(-0.1, 2)$ to the saddle point $(0.1, 2)$ represents the traveling front.

3.2. Phase portrait reduction of the three-component model. The traveling-wave equations for the original three-component model read

$$(3.15) \quad (-R_f c_0 + v)S_{0,\xi} = -\frac{MA_0S_0}{K_A K_S G(A_0, S_0)},$$

$$(3.16) \quad (-c_0 + v)A_{0,\xi} = -\gamma \frac{M}{K_A K_S G(A_0, S_0)},$$

$$(3.17) \quad c_0 M_{0,\xi} = -\frac{YMA_0S_0}{K_A K_S G(A_0, S_0)} + b(M_0 - M_b),$$

where $G(A, S)$ is given by (2.9). As for the two-component model, we use the conservation form to reduce the first two equations to

$$(3.18) \quad w'_0 = -\frac{\tilde{\epsilon}R_f(\gamma R_f S_+ + A_-)}{v(\gamma S_+ + A_-)}(w_0 - \gamma S_+)(w_0 + A_-)M/G(w_0),$$

and we rewrite (3.17) in terms of w_0 (by (2.5) and (3.4)) as

$$(3.19) \quad c_0 M'_0 = b(M_0 - M_b) + \frac{Y S_+ A_-}{K_A K_S (A_- + \gamma S_+)^2} (w_0 - \gamma S_+) (w_0 + A_-) M_0 / G(w_0).$$

Now (3.18)–(3.19) is a two-by-two ODE system amenable to phase portrait analysis. There are two equilibria, $(-A_-, M_b)$ and $(\gamma S_+, M_b)$. Forward in ξ , the first one $(-A_-, M_b)$ is an unstable node and the second one is a saddle. Hence, there is a unique path going from the node (source) to the saddle (sink) on the (w_0, M_0) phase plane.

See the phase plane portrait Figure 1 on the system

$$(3.20) \quad \begin{aligned} w' &= -200(w - 0.1)(w + 0.1)m, \\ m' &= 0.2(m - 2) + 200(w - 0.1)(w + 0.1)m, \end{aligned}$$

where the horizontal axis is on $w \in [-0.4, 0.4]$ and the vertical axis is on $m \in [0, 4]$. Only the part of the figure where $m \geq 2$ is meaningful for us. The orbit connecting the unstable node $(-0.1, 2)$ to the saddle $(0.1, 2)$ is the traveling-front solution.

4. Stability of traveling fronts. We analyze the stability of the explicit fronts in the two-component ND model. As in the Broadwell model, the analysis is done by using the energy method [10] based on the monotonicity property (3.11)–(3.12) and the conservative form of the (2.6). Our stability result is as follows.

THEOREM 4.1. *Consider (3.1)–(3.2) with the initial data $(u_0 + U_0, w_0 + W_0)$, where (u_0, w_0) is a traveling front. Suppose that the initial perturbation $(U_0, W_0) \in (H^1(R^1))^2$ and that $\int_{-\infty}^x U_0(x) dx \in L^2(R^1)$. It follows that $\int_{R^1} U_0 = 0$. Writing $(u, w)(\xi, t) = (u_0(\xi) + U(\xi, t), w_0(\xi) + W(\xi, t))$, $\xi = x - ct$. Then there exists a positive number δ depending only on (u_0, w_0) and the coefficients of the system such that if $\|(U_0, W_0)\|_{H^1} \leq \delta$ and that if*

$$(4.1) \quad (R_f - 1)^2 \leq \frac{7}{256} \frac{(\min\{\gamma R_f S_+, A_-\})^2}{\gamma R_f A_- S_+} \cdot \min \left\{ \frac{S_+ A_- \gamma}{R_f (\gamma S_+ - R_f^{-1} A_-)^2}, R_f - 1 \right\},$$

we have unique global in time solution $(U, W) \in L^\infty([0, \infty); (H^1)^2)$. Moreover,

$$\lim_{t \rightarrow \infty} \|(U, W)\|_{H^1} = \lim_{t \rightarrow \infty} \|(U, W)\|_{L^\infty} = 0.$$

REMARK 4.1. *Notice that (4.1) is independent of $\tilde{\gamma}$ and is invariant under the scaling change $(S_+, A_-) \rightarrow \lambda(S_+, A_-)$ for all $\lambda > 0$. Hence, it is equally valid for large boundary data. For any fixed (S_+, A_-, γ) , (4.1) requires that R_f be not too much larger than one. Also for any fixed (S_+, A_-, R_f) , (4.1) implies that γ be away from zero and infinity.*

To show stability, let us go to the moving-frame coordinate $\xi = x - c_0 t$, $t = t$, and write (2.6)–(2.7) as

$$(4.2) \quad u_t - c_0 u_\xi + v w_\xi = 0,$$

$$(4.3) \quad w_t - c_0 w_\xi + v((1 + R_f^{-1})w - R_f^{-1}u)_\xi = \tilde{\gamma}(u - w)(u - R_f w).$$

Write (u, w) as $(u, w) = (u_0(\xi) + U(\xi, t), w_0(\xi) + W(\xi, t))$ and put (4.2)–(4.3) into

$$(4.4) \quad U_t - c_0 U_\xi + v W_\xi = 0,$$

$$(4.5) \quad \begin{aligned} W_t + (v(1 + R_f^{-1}) - c_0)W_\xi - vR_f^{-1}U_\xi &= \tilde{\gamma}[(u_0 - R_f w_0)(U - W) \\ &+ (u_0 - w_0)(U - R_f W) + (U - R_f W)(U - W)]. \end{aligned}$$

By our assumption, $(U(\xi, 0), W(\xi, 0)) \in (H^1)^2$ and $\int_{-\infty}^{\xi} U(\xi', 0)d\xi' \in L^2$; it follows from the conservation law (4.4) that

$$\int_{-\infty}^{\infty} U(\xi, t)d\xi \equiv 0 \quad \forall t \geq 0.$$

Let $\Phi(\xi, t) = \int_{-\infty}^{\xi} U(\xi', t)d\xi'$, so $\Phi_{\xi} = U(\xi, t)$, and (4.4) reads

$$\Phi_{\xi,t} - c_0\Phi_{\xi\xi} + vW_{\xi} = 0,$$

which gives upon integrating in ξ

$$(4.6) \quad \Phi_t - c_0\Phi_{\xi} + vW = 0.$$

Substituting (4.6) into (4.5) yields

$$\begin{aligned} &(-v^{-1})(\partial_t - c_0\partial_{\xi})\Phi_t + (-v^{-1})(v(1 + R_f^{-1}) - c_0)((\partial_t - c_0\partial_{\xi})\Phi_{\xi}) - vR_f^{-1}\Phi_{\xi,\xi} \\ &= \tilde{\gamma}(u_0 - R_f w_0)(\Phi_{\xi} + v^{-1}(\partial_t - c_0\partial_{\xi})\Phi) \\ &+ \tilde{\gamma}(u_0 - w_0)(\Phi_{\xi} + R_f v^{-1}(\partial_t - c_0\partial_{\xi})\Phi) \\ (4.7) \quad &+ \Gamma(\Phi_{\xi}, \Phi_t - c_0\Phi_{\xi}), \end{aligned}$$

where Γ is quadratic. Let us write (4.7) as

$$\begin{aligned} &(\partial_t - c_0\partial_{\xi})^2\Phi + v(1 + R_f^{-1})(\partial_t - c_0\partial_{\xi})\Phi_{\xi} + v^2R_f^{-1}\Phi_{\xi,\xi} \\ (4.8) \quad &+ v\tilde{\gamma}Q(\xi)\Phi_{\xi} + \tilde{\gamma}P(\xi)\Phi_t = -v\Gamma(\Phi_{\xi}, \Phi_t - c_0\Phi_{\xi}), \end{aligned}$$

where

$$\begin{aligned} Q(\xi) &= (u_0 - R_f w_0)(1 - c_0v^{-1}) + (u_0 - w_0)(1 - c_0v^{-1}R_f), \\ (4.9) \quad P(\xi) &= (u_0 - R_f w_0) + R_f(u_0 - w_0). \end{aligned}$$

Because $c_0 \in (vR_f^{-1}, v)$ and $(u_0 - R_f w_0), (w_0 - u_0)$ are nonincreasing, there is a positive constant $\underline{P} = \underline{P}(u_0, w_0)$ such that

$$(4.10) \quad Q'(\xi) < 0, \quad P(\xi) \geq \underline{P} > 0.$$

Equation (4.8) is a damped semilinear wave equation; in the appendix we show the decay of solutions using the energy method to complete the proof.

5. WKB analysis of front perturbations. The stability theorem of section 4 seems to be restrictive. Here we perform formal WKB analysis to show that fronts are stable in the small damping regime for the two-component, ND model even without condition (4.1). Similar analysis extends to the original three-component system, predicting qualitatively the occurrence of front oscillations that are due to the biomass kinetics (namely M obeys a time-dependent ODE (1.3) and is not given by equilibrium 2.18). These formal results agree with our numerical experiments reported in section 6.

5.1. Damping in the nutrient-deficient model. Let us recall (4.8) for front perturbation:

$$(5.1) \quad (\partial_t - c_0 \partial_\xi)^2 \Phi + v(1 + R_f^{-1})(\partial_t - c_0 \partial_\xi) \Phi_\xi + v^2 R_f^{-1} \Phi_{\xi, \xi} + v \tilde{\gamma} Q(\xi) \Phi_\xi + \tilde{\gamma} P(\xi) \Phi_t = -v \Gamma(\Phi_\xi, \Phi_t - c_0 \Phi_\xi).$$

Since we will be concerned with small perturbations, let us omit the nonlinear terms on the right side and consider the linear equation

$$(5.2) \quad L\Phi \equiv (\partial_t - c_0 \partial_\xi)^2 \Phi + v(1 + R_f^{-1})(\partial_t - c_0 \partial_\xi) \Phi_\xi + v^2 R_f^{-1} \Phi_{\xi, \xi} + v \tilde{\gamma} Q(\xi) \Phi_\xi + \tilde{\gamma} P(\xi) \Phi_t = 0.$$

The first three terms of (5.2) form a wave operator and the last two terms give rise to damping. Let us consider the small damping limit, $\tilde{\gamma} \ll 1$, and the WKB ansatz of the solution as discussed by Whitham [21]:

$$(5.3) \quad \Phi(\xi, t) \sim a(X, \tau) \exp\{ik(t + \tilde{\gamma}^{-1} \Theta(X))\} + \dots,$$

where $X = \tilde{\gamma} \xi$, $\tau = \tilde{\gamma} t$ are slow space-time scales. Note that for small $\tilde{\gamma}$, the unperturbed fronts $(A_0, S_0) = (A_0, S_0)(X)$. The first and second derivatives of Φ are

$$\Phi_t \sim (\tilde{\gamma} a_\tau + ika) \exp\{ik(t + \tilde{\gamma}^{-1} \Theta(X))\},$$

$$\Phi_\xi \sim (\tilde{\gamma} a_X + ik \Theta_X a) \exp\{ik(t + \tilde{\gamma}^{-1} \Theta(X))\},$$

$$\Phi_{tt} \sim \{\tilde{\gamma}^2 a_{\tau\tau} + 2ik\tilde{\gamma} a_\tau - k^2 a\} \exp\{ik(t + \tilde{\gamma}^{-1} \Theta(X))\},$$

$$\Phi_{\xi\xi} \sim \{\tilde{\gamma}^2 a_{XX} + ik\tilde{\gamma} \Theta_{XX} a + 2\tilde{\gamma} ika_X \Theta_X - k^2 \Theta_X^2 a\} \exp\{ik(t + \tilde{\gamma}^{-1} \Theta(X))\},$$

$$(5.4) \quad \Phi_{t\xi} \sim \{\tilde{\gamma}^2 a_{\tau X} + \tilde{\gamma} ika_X + (\tilde{\gamma} a_\tau + ika)(ik \Theta_X)\} \exp\{ik(t + \tilde{\gamma}^{-1} \Theta(X))\}.$$

We can write (5.2) as

$$(5.5) \quad \Phi_{tt} + (v(1 + R_f^{-1}) - 2c_0) \Phi_{t\xi} + (c_0 - v)(c_0 - vR_f^{-1}) \Phi_{\xi\xi} + v\tilde{\gamma} Q(X) \Phi_\xi + vP(X) \Phi_t = 0.$$

Plugging (5.4) into (5.5) and collecting $O(1)$ terms, we have the eikonal equation

$$-k^2 a - k^2 a \Theta_X (v(1 + R_f^{-1}) - 2c_0) + (c_0 - v)(c_0 - vR_f^{-1})(-k^2 a \Theta_X^2) = 0,$$

or

$$1 + (v(1 + R_f^{-1}) - 2c_0) \Theta_X + (c_0 - v)(c_0 - vR_f^{-1}) \Theta_X^2 = 0,$$

which factors to give

$$(5.6) \quad \Theta_X = (c_0 - v)^{-1} \text{ or } (c_0 - R_f^{-1}v)^{-1},$$

showing that the phase $\Theta = (c_0 - v)^{-1} X$ or $(c_0 - R_f^{-1}v)^{-1} X$. The phase velocity is $(v - c_0)$ or $R_f^{-1}v - c_0$ for right (faster than front speed c_0) and left (slower than front speed c_0) moving perturbations. At order $O(\tilde{\gamma})$, we get the transport equation

$$2ika_\tau + (v(1 + R_f^{-1}) - 2c_0)(ika_X + ika_\tau \Theta_X)$$

$$+ (c_0 - v)(c_0 - vR_f^{-1})(ik \Theta_{XX} a + 2ika_X \Theta_X)$$

$$+ vQ(X) ik \Theta_X a + P(X) ika = 0,$$

which simplifies to

$$(5.7) \quad \begin{aligned} & (2 + (v(1 + R_f^{-1}) - 2c_0)\Theta_X)a_\tau \\ & + (v(1 + R_f^{-1}) - 2c_0 + 2(c_0 - v)(c_0 - vR_f^{-1})\Theta_X)a_X \\ & + (vQ(X)\Theta_X + P(X))a = 0. \end{aligned}$$

In case $\Theta_X = (c_0 - v)^{-1}$, the coefficient of a_τ becomes

$$2 + (vR_f^{-1} - c_0 + v - c_0)(c_0 - v)^{-1} = 1 + \frac{c_0 - vR_f^{-1}}{v - c_0} = \frac{v(1 - R_f^{-1})}{v - c_0};$$

that of a_X is equal to

$$v(1 + R_f^{-1}) - 2c_0 + 2(c_0 - vR_f^{-1}) = v(1 - R_f^{-1});$$

and that of a reduces to

$$(5.8) \quad \begin{aligned} & vQ(X)\Theta_X + P(X) \\ & = \frac{v}{c_0 - v} \left((u_0 - R_f w_0) \frac{v - c_0}{v} + (u_0 - w_0)(1 - c_0 v^{-1} R_f) \right) \\ & \quad + (u_0 - R_f w_0) + R_f(u_0 - w_0) \\ & = (u_0 - w_0) \left(\frac{v}{c_0 - v} (1 - c_0 v^{-1} R_f) + R_f \right) \\ & = (u_0 - w_0) \frac{v(1 - R_f)}{c_0 - v} = S_0 \gamma (R_f - 1)^2 \frac{v}{v - c_0}. \end{aligned}$$

Therefore, (5.7) reduces to

$$(5.9) \quad a_\tau + (v - c_0)a_X + \gamma R_f (R_f - 1) S_0(X) a = 0.$$

The damping coefficient is $\gamma R_f (R_f - 1) S_0(X)$. Since $S_0(X)$ is a monotone increasing function from zero at $X = -\infty$ to S_+ at $X = +\infty$, we see that *for faster ($> c_0$) moving perturbation, there is more damping to the right of the front (at $X = 0$) than to the left.*

In case $\Theta = (c_0 - R_f^{-1}v)^{-1}X$, the three consecutive coefficients in the transport equation are

$$2 + (v(1 + R_f^{-1}) - 2c_0) \frac{1}{c_0 - vR_f^{-1}} = \frac{v(1 - R_f^{-1})}{c_0 - vR_f^{-1}},$$

$$v(1 + R_f^{-1}) - 2c_0 + 2(c_0 - v) = v(R_f^{-1} - 1),$$

and

$$(5.10) \quad \begin{aligned} & vQ(X)\Theta_X + P(X) \\ & = \frac{v}{c_0 - vR_f^{-1}} \left((u_0 - R_f w_0) \frac{v - c_0}{v} + (u_0 - w_0)(1 - c_0 v^{-1} R_f) \right) \\ & \quad + (u_0 - R_f w_0) + R_f(u_0 - w_0) \\ & = \left(\frac{v - c_0}{c_0 - vR_f^{-1}} + 1 \right) (u_0 - R_f w_0) = \frac{v(1 - R_f^{-1})}{c_0 - vR_f^{-1}} (u_0 - R_f w_0). \end{aligned}$$

The transport equation eventually becomes

$$(5.11) \quad a_\tau - (c_0 - R_f^{-1}v)a_X + (R_f - 1)A_0(X)a = 0.$$

Since A_0 decreases from A_- at $\xi = -\infty$ to zero at $\xi = +\infty$, we see that *for more slowly ($< c_0$) moving perturbation, there is more damping to the left of the front (at $X = 0$) than to the right.*

In any event, the front perturbations always get damped in the ND model. The larger the R_f and γ , the more damping. The same analysis also shows that front damping is always present in the general two-component model for any positive and finite K_A and K_S .

5.2. Oscillations in the three-component model. Now let us consider the original three-equation model, which includes the biomass kinetic effect. The conservative form of the system is

$$(5.12) \quad u_t + vw_x = 0,$$

$$(5.13) \quad w_t + v((1 + R_f^{-1})w - R_f^{-1}u)_x = \frac{\epsilon(u - w)(u - R_f w)M}{(1 + K_A^{-1}A)(1 + K_S^{-1}S)},$$

$$(5.14) \quad M_t = -b(M - M_b) + \frac{YASM}{(K_A + A)(K_S + S)},$$

where $\epsilon = R_f^{-1}(R_f - 1)^{-1}(K_A K_S)^{-1}$. Linearizing about the traveling front (S_0, A_0, M_0) and denoting the perturbation by (S, A, m) , we have the system

$$(5.15) \quad L_\epsilon \Phi + \epsilon v(u_0 - w_0)(u_0 - R_f w_0) \left[\begin{aligned} & \frac{m}{(1 + K_A^{-1}A_0)(1 + K_S^{-1}S_0)} \\ & - \frac{M_0 K_A^{-1}A}{(1 + K_A^{-1}A_0)^2(1 + K_S^{-1}S_0)} \\ & - \frac{M_0 K_S^{-1}S}{(1 + K_A^{-1}A_0)(1 + K_S^{-1}S_0)^2} \end{aligned} \right] = 0$$

and

$$(5.16) \quad m_t - c_0 m_\xi = -bm + \frac{Y}{K_A K_S} \left[\begin{aligned} & \frac{A_0 S_0 m}{(1 + K_A^{-1}A_0)(1 + K_S^{-1}S_0)} \\ & + \frac{M_0 S_0 A}{(1 + K_A^{-1}A_0)(1 + K_S^{-1}S_0)} \\ & + \frac{S A_0 M_0}{(1 + K_A^{-1}A_0)(1 + K_S^{-1}S_0)} \end{aligned} \right] \\ - \frac{Y M_0 A_0 S_0}{K_A K_S} \left[\begin{aligned} & \frac{K_A^{-1}A}{(1 + K_A^{-1}A_0)^2(1 + K_S^{-1}S_0)} \\ & + \frac{K_S^{-1}S}{(1 + K_A^{-1}A_0)(1 + K_S^{-1}S_0)^2} \end{aligned} \right],$$

where the operator L_ϵ is

$$L_\epsilon \Phi = (\partial_t - c_0 \partial_\xi)^2 \Phi + v(1 + R_f^{-1})(\partial_t - c_0 \partial_\xi) \Phi_\xi + v^2 R_f^{-1} \Phi_{\xi, \xi}$$

$$(5.17) \quad + \frac{\epsilon M_0}{(1 + K_A^{-1}A_0)(1 + K_S^{-1}S_0)}(vQ\Phi_\xi + P\Phi_t).$$

For small ϵ , (S_0, A_0, M_0) depends on ξ slowly and can be thought of as mainly depending on the slow variable $\epsilon\xi$. For the coming WKB analysis, we assume that M_0 is a bounded function uniform in ϵ .

Let us consider WKB ansatz of the form

$$(5.18) \quad \begin{aligned} \Phi &\sim a(X, \tau) \exp\{ik(t + \epsilon^{-1}\Theta(X))\} + \dots, \\ m &\sim \bar{m}(X, \tau) \exp\{ik(t + \epsilon^{-1}\Theta(X))\} + \dots, \end{aligned}$$

where $X = \epsilon\xi$, $\tau = \epsilon t$, and (A_0, S_0, M_0) depend slowly on ξ (through X).

At leading order $O(1)$, the eikonal equation on Θ is still (5.6). The m equation reads

$$(5.19) \quad \begin{aligned} ik\bar{m}(1 - c_0\Theta_X) &= \left(-b + \frac{YA_0S_0}{(K_A + A_0)(K_S + S_0)}\right) \bar{m} \\ &+ \frac{YM_0}{(K_A + A_0)(K_S + S_0)}(AS_0 + SA_0) \\ &- YM_0A_0S_0 \left(\frac{A}{(K_A + A_0)^2(K_S + S_0)} + \frac{S}{(K_A + A_0)(K_S + S_0)^2}\right), \end{aligned}$$

which simplifies to

$$(5.20) \quad \begin{aligned} &\left[ik(1 - c_0\Theta_X) + \left(b - \frac{YA_0S_0}{(K_A + A_0)(K_S + S_0)}\right) \right] \bar{m} \\ &= \frac{YM_0}{(K_A + A_0)(K_S + S_0)} \left[\frac{AK_AS_0}{K_A + A_0} + \frac{A_0K_S S}{K_S + S_0} \right]. \end{aligned}$$

Recall that $U = \Phi_\xi$, $W = (-v^{-1})(\Phi_t - c_0\Phi_\xi)$; therefore,

$$(5.21) \quad \begin{aligned} A &= (R_f - 1)^{-1}(U - R_fW) = (R_f - 1)^{-1}(R_fv^{-1}\Phi_t + (1 - R_fv^{-1}c_0)\Phi_\xi) \\ &= (ika)(R_f - 1)^{-1}(R_fv^{-1} + (1 - R_fv^{-1}c_0)\Theta_X), \end{aligned}$$

$$(5.22) \quad \begin{aligned} S &= \gamma^{-1}(R_f - 1)^{-1}(U - W) = \gamma^{-1}(R_f - 1)^{-1}(v^{-1}\Phi_t + (1 - v^{-1}c_0)\Phi_\xi) \\ &= (ika)\gamma^{-1}(R_f - 1)^{-1}(v^{-1} + (1 - v^{-1}c_0)\Theta_X). \end{aligned}$$

Combining (5.19)–(5.22), we have

$$(5.23) \quad \begin{aligned} &\left[(1 - c_0\Theta_X) + (ik)^{-1} \left(b - \frac{YA_0S_0}{(K_A + A_0)(K_S + S_0)}\right) \right] \bar{m} \\ &= \frac{aYM_0}{(K_A + A_0)(K_S + S_0)} \left[\frac{K_AS_0}{K_A + A_0} (R_f - 1)^{-1}(R_fv^{-1} + (1 - R_fv^{-1}c_0)\Theta_X) \right. \\ &\quad \left. + \frac{A_0K_S}{K_S + S_0} \gamma^{-1}(R_f - 1)^{-1}(v^{-1} + (1 - v^{-1}c_0)\Theta_X) \right]. \end{aligned}$$

At $O(\epsilon)$, we get the transport equation

$$ik \left[(2 + (v(1 + R_f^{-1}) - 2c_0)\Theta_X)a_\tau + \frac{M_0K_AK_S(vQ(X)\Theta_X + P(X))}{(K_A + A_0)(K_S + S_0)}a \right]$$

$$\begin{aligned}
 & + (v(1 + R_f^{-1}) - 2c_0 + 2(c_0 - v)(c_0 - vR_f^{-1})\Theta_X)a_X \Big] \\
 & + v(u_0 - w_0)(u_0 - R_f w_0) \left[\frac{\bar{m}}{(1 + K_A^{-1}A_0)(1 + K_S^{-1}S_0)} \right. \\
 & \qquad - \frac{M_0 K_A^{-1}A}{(1 + K_A^{-1}A_0)^2(1 + K_S^{-1}S_0)} \\
 & \qquad \left. - \frac{M_0 K_S^{-1}S}{(1 + K_A^{-1}A_0)(1 + K_S^{-1}S_0)^2} \right] = 0.
 \end{aligned}
 \tag{5.24}$$

If $\Theta_X = (c_0 - v)^{-1}$, we get from (5.23) that

$$\left(\frac{v}{v - c_0} + (ik)^{-1} \left(b - \frac{Y A_0 S_0}{(K_A + A_0)(K_S + S_0)} \right) \right) \bar{m} = \frac{Y a M_0}{(K_A + A_0)^2 (K_S + S_0)} \frac{K_A S_0}{v - c_0};$$

therefore,

$$(5.25) \quad v\bar{m} = \frac{Y S_0 K_A M_0 a}{(K_A + A_0)^2 (K_S + S_0) \left(1 + \frac{v - c_0}{v} (ik)^{-1} \left(b - \frac{Y A_0 S_0}{(K_A + A_0)(K_S + S_0)} \right) \right)}.$$

Similarly, if $\Theta_X = (c_0 - vR_f^{-1})^{-1}$, we have

$$(5.26) \quad v\bar{m} = \frac{-Y A_0 K_S M_0 a \gamma^{-1}}{(K_A + A_0)(K_S + S_0)^2 \left(1 - \frac{c_0 R_f - v}{v} (ik)^{-1} \left(b - \frac{Y A_0 S_0}{(K_A + A_0)(K_S + S_0)} \right) \right)}.$$

Notice that the terms in the first bracket of (5.24) are same as those computed in the last subsection. Taking $\Theta_X = (c_0 - v)^{-1}$, we get from (5.21) and (5.22) that $A = \frac{ika}{v - c_0}$, $S = 0$. It follows from (5.24) and (5.25) that

$$\begin{aligned}
 & v(1 - R_f^{-1})(v - c_0)^{-1}a_\tau + v(1 - R_f^{-1})a_X \\
 & + \frac{K_A K_S M_0}{(K_A + A_0)(K_S + S_0)} \frac{v\gamma}{v - c_0} (R_f - 1)^2 S_0 a \\
 & + a(ik)^{-1} \frac{(u_0 - w_0)(u_0 - R_f w_0) Y S_0 M_0 K_A}{(1 + K_A^{-1}A_0)(1 + K_S^{-1}S_0)(K_A + A_0)^2 (K_S + S_0)} \\
 & \times \left(1 + \frac{v - c_0}{v} (ik)^{-1} \left(b - \frac{Y A_0 S_0}{(K_A + A_0)(K_S + S_0)} \right) \right)^{-1} \\
 & - a \frac{v}{v - c_0} \frac{(u_0 - w_0)(u_0 - R_f w_0) M_0 K_A^{-1}}{(1 + K_A^{-1}A_0)^2 (1 + K_S^{-1}S_0)} = 0.
 \end{aligned}
 \tag{5.27}$$

Equation (5.27) can be written as

$$(5.28) \quad a_\tau + (v - c_0)a_X + (G_d + iO_s)a = 0,$$

where

$$\begin{aligned}
 G_d = & \frac{K_A K_S \gamma R_f (R_f - 1)(M_0 S_0)}{(K_A + A_0)(K_S + S_0)} - \frac{K_A K_S \gamma R_f (R_f - 1)(A_0 M_0 S_0)}{(K_A + A_0)^2 (K_S + S_0)} \\
 & + \frac{(v - c_0)^2 K_A^2 K_S \gamma R_f (R_f - 1)(A_0 M_0 S_0^2) Y \left(b - \frac{Y A_0 S_0}{(K_A + A_0)(K_S + S_0)} \right)}{v^2 (K_A + A_0)^3 (K_S + S_0)^2 \left(k^2 + \left(b - \frac{Y A_0 S_0}{(K_A + A_0)(K_S + S_0)} \right)^2 \left(\frac{v - c_0}{v} \right)^2 \right)},
 \end{aligned}
 \tag{5.29}$$

$$(5.30) \quad O_s = \frac{c_0 - v}{v} \frac{R_f(R_f - 1)\gamma K_A^2 K_S Y (A_0 M_0 S_0^2) k}{(K_A + A_0)^3 (K_S + S_0)^2 \left(k^2 + \left(b - \frac{Y A_0 S_0}{(K_A + A_0)(K_S + S_0)} \right)^2 \left(\frac{v - c_0}{v} \right)^2 \right)}.$$

We see that to have front oscillation or instability, we must have $G_d \leq 0$; then O_s gives the oscillation frequency. In the case of (5.28), the advection velocity $c_0 - v$ should also be near zero to have steady oscillation in the moving frame. This is the case if R_f is close to one, implying that $K_A, K_S \gg 1$ to keep ϵ small. Even if K_A and K_S are large, they balance in each of the three terms of G_d in (5.29). Near the frontal region, we assume that A_0, S_0 are of the same $O(1)$. We further calculate

$$(5.31) \quad G_d = \frac{K_A K_S \gamma R_f (R_f - 1) M_0 S_0 K_A}{(K_A + A_0)^2 (K_S + S_0)} + \frac{K_A^2 K_S \gamma R_f (R_f - 1) (A_0 M_0 S_0^2) Y \left(b - \frac{Y A_0 S_0}{(K_A + A_0)(K_S + S_0)} \right)}{(K_A + A_0)^3 (K_S + S_0)^2 \left(\tilde{k}^2 + \left(b - \frac{Y A_0 S_0}{(K_A + A_0)(K_S + S_0)} \right)^2 \right)},$$

where $\tilde{k} = k(v - c_0)^{-1}v$. For $k = O(1)$, $\tilde{k} = O((R_f - 1)^{-1})$. We see that to avoid damping, we must have

$$(5.32) \quad \tilde{b} \equiv b - y \equiv b - \frac{Y A_0 S_0}{(K_A + A_0)(K_S + S_0)} < 0;$$

otherwise, $G_d > 0$. For large Y , y is nearly $K_A^{-1} K_S^{-1} Y$. Let us now write G_d as

$$(5.33) \quad \begin{aligned} G_d &= \frac{K_A^2 K_S \gamma R_f (R_f - 1) M_0 S_0}{(K_A + A_0)^2 (K_S + S_0)} \left(1 + \frac{y \tilde{b}}{\tilde{k}^2 + \tilde{b}^2} \right) \\ &= \gamma M_0 O(R_f - 1) \left(1 + \frac{y(b - y)}{\tilde{k}^2 + (b - y)^2} \right) \\ &= \gamma M_0 O(R_f - 1) \frac{\tilde{k}^2 + b(b - y)}{\tilde{k}^2 + (b - y)^2}. \end{aligned}$$

If we take $y - b = 2b^{-1}\tilde{k}^2 = O((R_f - 1)^{-2})$, then

$$(5.34) \quad \begin{aligned} G_d &= \gamma M_0 O(R_f - 1) \frac{b(b - y)}{2(0.5b(y - b) + (y - b)^2)} \\ &= -\gamma M_0 O(R_f - 1) O((y - b)^{-1}) = -O(\gamma M_0 (R_f - 1)^3) < 0, \end{aligned}$$

giving rise to growth or growth-induced oscillation. The oscillation frequency is now expressed as

$$(5.35) \quad \begin{aligned} O_s &= \frac{R_f(R_f - 1)\gamma K_A^2 K_S M_0 S_0 y \tilde{k}}{(K_A + A_0)^2 (K_S + S_0)(\tilde{k}^2 + (b - y)^2)} \\ &= O(\gamma M_0 (R_f - 1) y^{-1} \tilde{k}) = O(\gamma M_0 (R_f - 1)^2), \end{aligned}$$

which is fairly small except when M_0 happens to be large.

This regime is observed numerically to support biomass growth during an initial transient period (see section 6).

Now if $\Theta_X = (c_0 - vR_f^{-1})^{-1}$, combining (5.24) and (5.26), we arrive at a similar transport equation:

$$(5.36) \quad a_\tau + (vR_f^{-1} - c_0)a_X + (G_d + iO_s)a = 0,$$

where

$$(5.37) \quad G_d = \frac{K_A K_S (R_f - 1)(M_0 A_0)}{(K_A + A_0)(K_S + S_0)} - \frac{K_A K_S (R_f - 1)(A_0 M_0 S_0)}{(K_A + A_0)(K_S + S_0)^2} + \frac{K_A K_S^2 (R_f - 1) A_0^2 M_0 S_0 Y}{(K_A + A_0)^2 (K_S + S_0)^3} \frac{\left(b - \frac{Y A_0 S_0}{(K_A + A_0)(K_S + S_0)}\right) \left(\frac{c_0 R_f - v}{v}\right)^2}{k^2 + \left(b - \frac{Y A_0 S_0}{(K_A + A_0)(K_S + S_0)}\right)^2 \left(\frac{v - c_0 R_f}{v}\right)^2}$$

and where

$$(5.38) \quad O_s = \frac{(v - c_0 R_f)(R_f - 1) K_A K_S^2 A_0 M_0 y k}{v(K_A + A_0)(K_S + S_0)^2 \left(k^2 + \left(b - \frac{Y A_0 S_0}{(K_A + A_0)(K_S + S_0)}\right)^2 \left(\frac{v - c_0 R_f}{v}\right)^2\right)}.$$

For the advection velocity $vR_f^{-1} - c_0$ to be near zero, $R_f \gg 1$ is necessary. In the meantime, to make sure that each of the three terms in G_d of (5.37) is bounded as $R_f \rightarrow \infty$, we need to impose

$$(5.39) \quad O(K_A) = O(K_S) = O(R_f^{-\alpha}), \quad \alpha > 0, \quad -2\alpha + 1 \leq 0.$$

Now, for $\epsilon \ll 1$, we must also have $2\alpha - 2 < 0$. It follows that $\alpha \in [\frac{1}{2}, 1)$. We still use the notations \tilde{b} , \tilde{k} , y to calculate

$$(5.40) \quad G_d = \frac{K_A K_S^2 (R_f - 1) A_0 M_0}{(K_A + A_0)(K_S + S_0)^2} \left(1 + \frac{y(b - y)}{\tilde{k}^2 + (b - y)^2}\right) = O(K_A^3 M_0 R_f) \frac{\tilde{k}^2 + b(b - y)}{\tilde{k}^2 + (b - y)^2}.$$

Now $\tilde{k} = k(v - c_0 R_f)^{-1} v$, $k = O(1)$, and $\tilde{k} = O(1)$. Choosing $y - b = 2b^{-1} \tilde{k}^2 = O(1)$, we have from (5.40) that

$$(5.41) \quad G_d = -O(K_A^3 M_0 R_f) O(1) = -O(M_0 R_f^{-\beta}) < 0,$$

where $\beta \equiv 3\alpha - 1 \in [\frac{1}{2}, 2)$. The corresponding oscillation frequency is

$$(5.42) \quad O_s = O(R_f K_A^3 M_0) O\left(\frac{\tilde{k} y}{\tilde{k}^2 + (b - y)^2}\right) = O(M_0 R_f^{-\beta}),$$

giving the oscillation period

$$(5.43) \quad T = O(M_0^{-1} R_f^\beta).$$

It is interesting that (5.43) is similar to (2.31), except that the exact value of β is not determined from our analysis.

The above regime is observed numerically to support temporal front oscillations for extended times (see section 6).

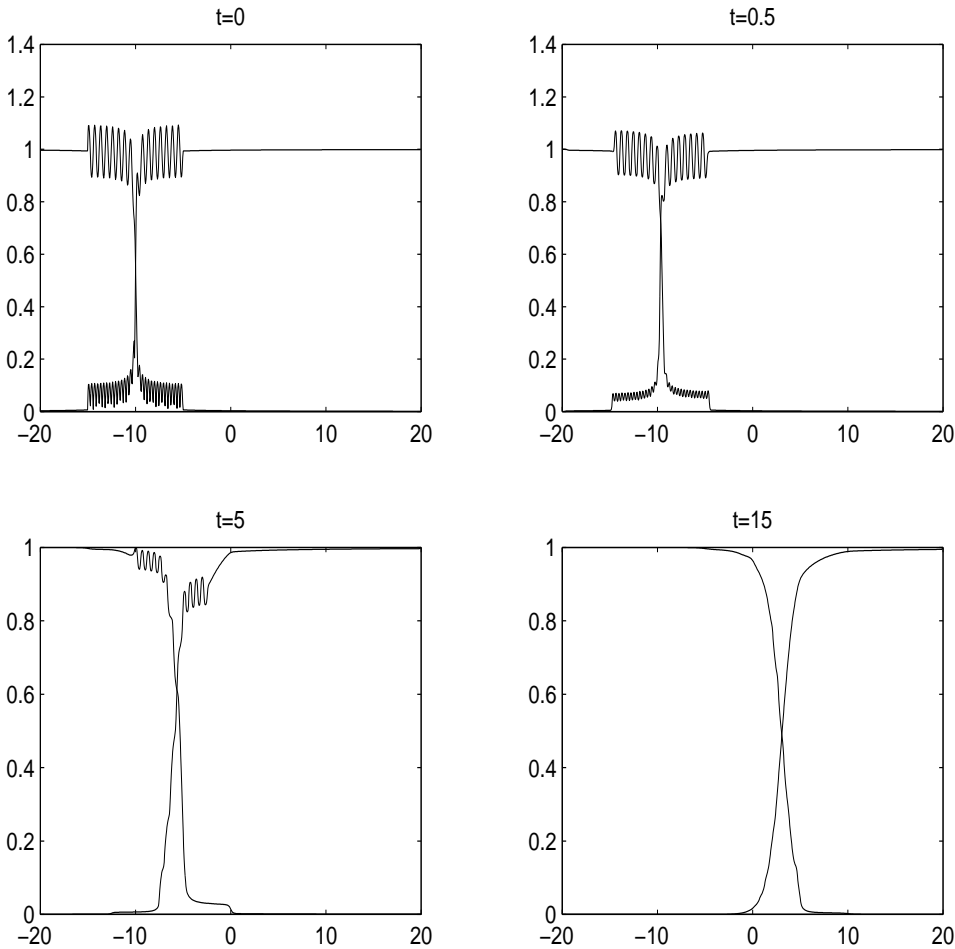


FIG. 2. An initial perturbation of the traveling fronts in the two-component model (6.1) will quickly disappear as the wave passes over the perturbation at times $t = 0, 0.5, 5, 15$.

6. Numerical results.

6.1. Nutrient-deficient model. We simulate the ND, two-equation model

$$(6.1) \quad \begin{aligned} R_f S_t - S_x &= -SA, \\ A_t - A_x &= -\gamma SA \end{aligned}$$

on the interval $[-20, 20]$. We use the standard second-order upwind scheme to discretize the advection terms and the Roe's Superbee limiter to compute sharp fronts also. See Leveque [12, Chapter 16] for details of this method. The reaction terms are treated explicitly.

In Figure 2 (top left) we show the initial data, the frontlike profiles of A and S with spatial perturbations which are localized oscillatory perturbations on the interval $[-15, -5]$ with amplitude 0.1. The parameters are $R_f = 2$, $\gamma = 0.2$, the spatial grid size = 0.05, and the time step = 0.025.

In Figure 2 (top right) we see that after a short evolution, at $t = 0.5$, the perturbation to the right (left) of the A (S) front quickly decays away. Here the A front

is the fast front and the S front is the slow front. This is just as the WKB theory predicted.

In Figure 2 (bottom left) the remaining perturbation still exists at $t = 5$, although weakened; however, at $t = 15$ (bottom right), the perturbation gets sucked completely into the fronts.

For this calculation we verified that reducing space and time steps by a factor of two does not change the results significantly.

6.2. Three-component model. We compare the full three-component biodegradation model (BM) in (2.1)–(2.3) with the general two-component equilibrium model (EM) in (2.25)–(2.26) and the ND model in (2.27)–(2.28) for the same parameters.

In our calculations we used the fourth-order-centered finite difference method for the spatial derivatives and a variable order, variable time step Adams–Bashforth–Moulton method in time. The time step and method order for the time integration method was varied to ensure that the time integration errors were below 10^{-6} . The number of spatial grid points was varied between 600 and 1000 to confirm that the solutions had converged to within an absolute error tolerance of 0.001. A small amount of artificial dissipation was included in the simulations by setting $D = 0.1 \times \Delta x$.

In the first regime we study, K_A and K_S are smaller than $O(A_-) = O(S_+) = 1$, and R_f is large, consistent with WKB (5.36)–(5.42). In the examples of this regime, we take $v = 1$, $K_A = 0.02$, $K_S = 0.04$, $\gamma = 0.4$, $Y = 0.1$, $M_b = 0.01$, $S_+ = A_- = 1$, and $D = 0$; and we will vary R_f and b . We take as the initial data

$$(6.2) \quad S(x, 0) = \frac{1}{2}S_+ \left(1 - \tanh \left[\frac{1}{4\pi}(x - 50) \right] \right),$$

$$(6.3) \quad A(x, 0) = A_-(S_+ - S(x, 0)),$$

and $M(x, 0)$ defined from the equilibrium by (2.18) when the solvability condition (2.17) is satisfied and $M(x, 0) = M_b$ otherwise.

In Figure 3 the solutions of the BM, EM, and ND are plotted at three time slices ($t = 0, 400, 800$) with waves moving to the right. Although the speeds are approximately equal (Figure 4), the profile of the solution of the ND model is much steeper than those of the other solutions. Note how the equilibrium M in Figure 3(b) closely tracks the M from the full three-equation model in Figure 3(a). Equally important is that the broad S and A profiles of the EM are much closer to those of the BM than the corresponding M profiles.

The solution of the ND in Figure 3(c) quickly converges to the traveling wave (3.4)–(3.5), $c_{ND} = 0.15556$, confirming its strong stability. The profiles are significantly different from the broader traveling-wave profiles of the two-component EM with the traveling wave velocity $c_{EM} = 0.15525$ (Figure 3(b)) or the BM, with traveling wave velocity $c_{BM} = 0.15525$ (Figure 3(a)). The difference in profiles is not unexpected, since both K_A and K_S are small (away from ND regime). Even though ND solutions are much steeper, they move at the same speed.

The velocity plots (Figure 4) show the relative rates of convergence to the traveling wave. The BM solution converges more slowly and oscillates about the traveling-wave velocity before settling down. The parameters above are near the limit of the solvability condition (2.17) with

$$(6.4) \quad 0.1 = b > \frac{YA_-S_+}{(K_A + A_-)(K_S + S_+)} = 0.09427,$$

where we expect the two models to be close.

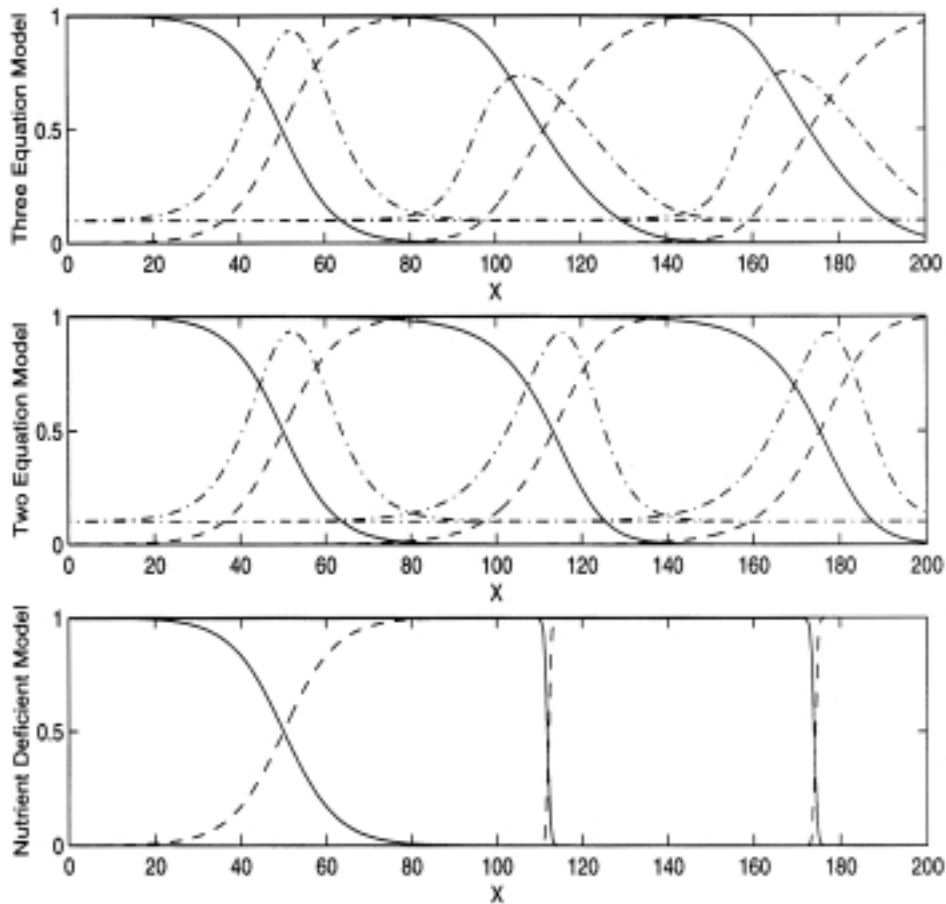


FIG. 3. The solutions of the three-equation model BM (a), EM (b), and ND (c) are plotted at three time slices ($t = 0, 400, 800$) with waves moving to the right. The solid curves are for A , the dashed curves are for S , the dot-dashed curves are for M , and the horizontal dot-dashed lines denote the background biomass M_b . The biomass M is magnified ten times so as to be seen on the same scale as the (A, S) profiles.

If b is made slightly smaller, the oscillations persist in the solution of the three-equation model and the solution becomes periodic. In this regime, the two-equilibrium-component model is no longer appropriate; however, the ND can still keep track of the mean value of the front velocity of the full three-equation model (in calculations not shown here).

When we reduce b to $b = 0.02$, the solution of the BM quickly converges to the periodic limit cycle shown in Figure 5. The biomass profile is right after the A profile at $t = 300$, lags behind at $t = 320$, catches up, and overtakes the front, only to lag behind again at $t = 380$. Figure 6(a) shows front locations in the reference frame of the ND traveling wave velocity, $c_{ND} = 0.15556$. The acceptor front A (solid line) oscillates less than the substrate S (dashed line), and both are ahead of the peak of the biomass M (dashed-dot line). These conditions are also evident in Figure 6(b) where the front velocities, A velocity (solid line) and S velocity (dashed line), oscillate about the traveling wave speed c_{ND} (dotted line).

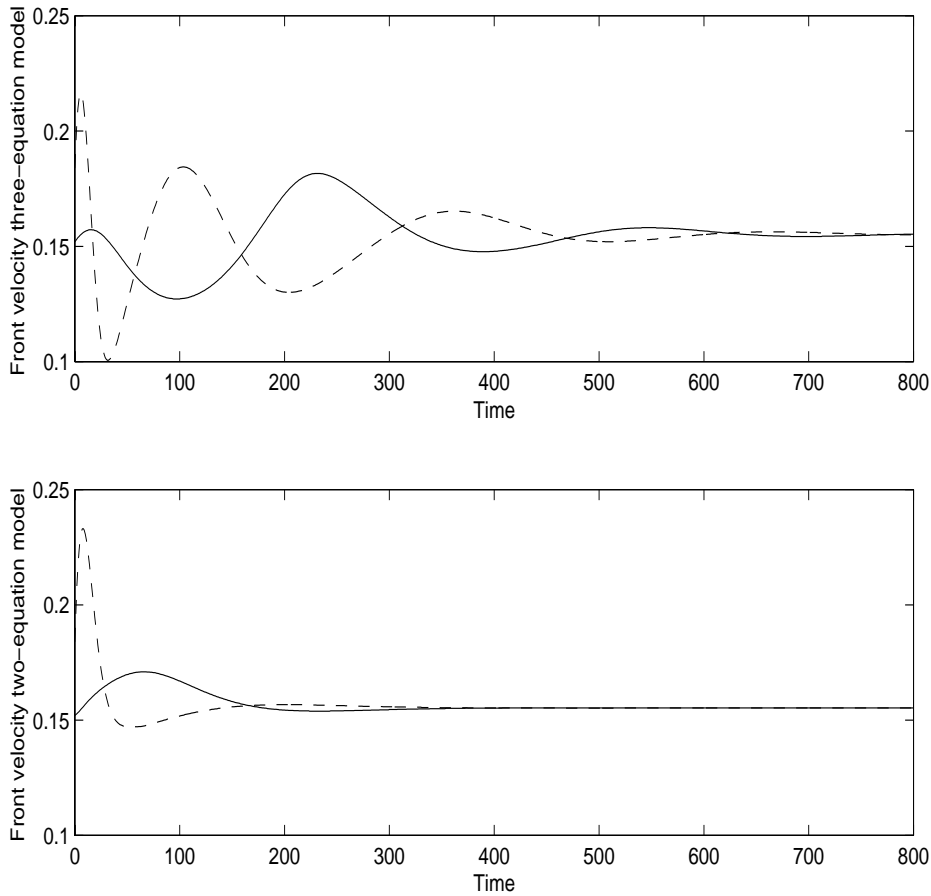


FIG. 4. Front velocity of A (solid line) and S (dashed line) vs. time for the BM (a) and EM (b) models with $b = 0.1$. The initial velocities quickly converge to a traveling wave velocity $\approx c_{ND} = 0.15556$ of the ND. The velocities are computed at the midpoint of the fronts where $A = \frac{1}{2}$ and $S = \frac{1}{2}$.

In Figure 7 the space-time density plot of the BAZ, characterized by the function

$$(6.5) \quad Z(A, S) = \frac{AS}{(K_A + A)(K_S + S)}$$

for the BM, shows how the reaction zone advances ahead of the fronts but cannot sustain itself. After the initial transient time, the reaction zone oscillates persistently.

Next, we keep $b = 0.02$ and study the parameter range $R_f = 1.5, 5, 8.5, 12$ (Figure 8). The maximum value of M increases from a steady value when $R_f = 1.5$ to higher and higher oscillatory values as R_f increases. Notice how the frequency is only weakly dependent on R_f in the time domain (Figure 8(a)), but because the fronts slow down at higher R_f , the increased frequency is dramatically evident in the spatial domain (Figure 8(b)). The period increases approximately linearly with R_f . This scaling is close to that of the exact solution in [19], or $\beta = 1$ in (5.43). The phenomenon that the larger the R_f the larger the oscillation period can be attributed to the fact that the A and S fronts have vastly disparate advection velocities and require a longer

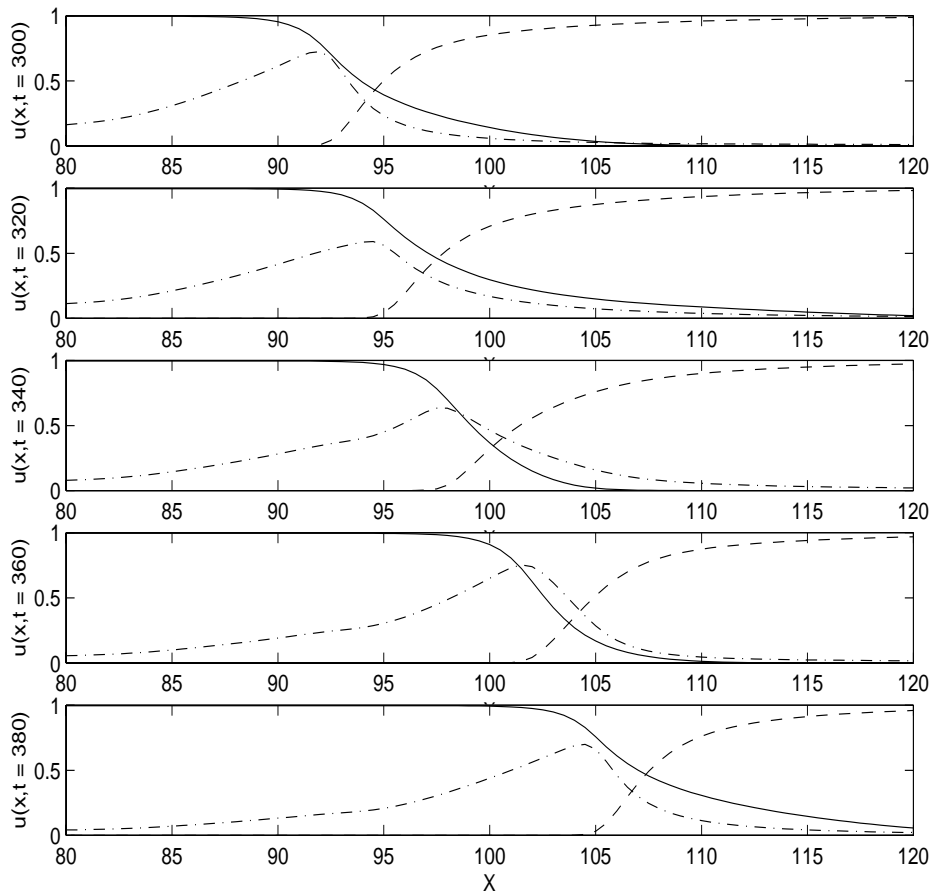


FIG. 5. The solution of the BM, shown at times $t = 300$ (top), 320, 340, 360, and 380 (bottom), with $b = 0.02$ violate the relaxation condition (6.4) and quickly converges to a limit cycle. The solid curves are for A , the dashed curves are for S , the dot-dashed curves are for M .

time to come together again.

In the second regime we study, Y is large, R_f is close to one, and $K_A = K_S$ are larger than $O(A_-) = O(S_+) = 1$. These conditions are consistent with the WKB analysis (5.28)–(5.35). We observe transient growth in biomass M and eventual saturation. We use the second-order upwind scheme for the A and S equations and the second-order Runge–Kutta scheme for the M equation. At each time step we find A and S first, then treat them as coefficients when updating the M . The method is explicit.

In Figures 9 and 10 $Y = 100$, $K_A = K_S = 10$, $b = 0.5$, $\gamma = 3$, and $R_f = 1.1$; and the initial data for M is $M_b = 0.4$. We illustrate in these two figures that the biomass growth is a transient phenomenon and it is saturated eventually. Figure 9 shows the profiles of the three components at $t = 20$ and $t = 100$. The biomass grows from $M_b = 0.4$ and attains the maximum near the place where the A and S overlap. If we view the solutions at $t = 20$ as a perturbation of that at $t = 100$, Figure 9 illustrates that the biomass profile can grow in a transient time period under perturbation. We see in Figure 10 that the biomass spatial maximum peaks then asymptotes to a constant.

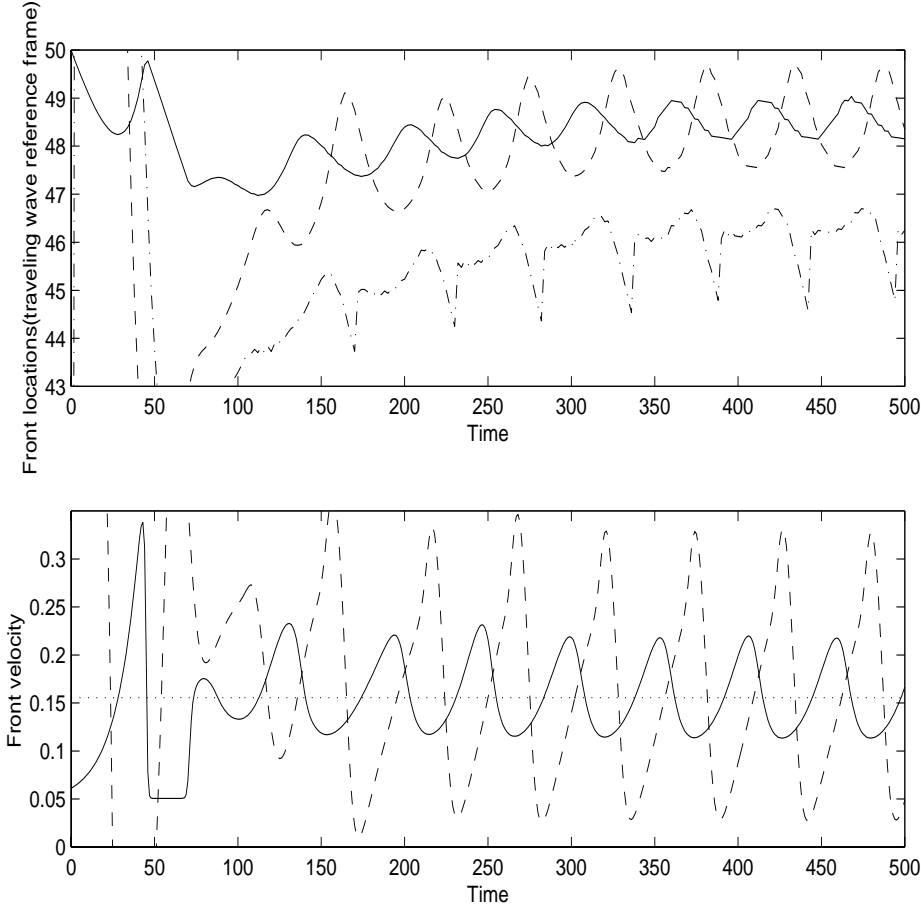


FIG. 6. Front oscillations occur when relaxation condition (6.4) is violated with $b = 0.02$. The front position (in the reference frame of the traveling wave) of the acceptor front A (solid line) oscillates less than the substrate S (dashed line) and both are ahead of the peak of the biomass M (dot-dashed line) in (a). This is also evident in (b), where the front velocities, A velocity (solid line) and S velocity (dashed line), oscillate about the traveling-wave speed c_{ND} (dotted line).

7. Appendix.

Proof of Theorem 4.1. Multiplying (4.8) by Φ_t and integrating over (x, t) to find \int is a shorthand for \int_{R^1} below:

$$\int_0^t \int \Phi_t \Phi_{tt} - \Phi_{t\xi} (c_0^2 - v(1 + R_f^{-1})c_0 + v^2 R_f^{-1}) \Phi_\xi + \int_0^t \int v \tilde{\gamma} Q(\xi) \Phi_t \Phi_\xi + \tilde{\gamma} P(\xi) \Phi_t^2 = -v \int_0^t \int \Phi_t \Gamma(\Phi_\xi, \Phi_t - c_0 \Phi_\xi),$$

or

$$\int_0^t \frac{d}{dt} \int \frac{1}{2} \Phi_t^2 + \frac{1}{2} (v - c_0) (c_0 - v R_f^{-1}) \Phi_\xi^2 + \int_0^t \int v \tilde{\gamma} Q(\xi) \Phi_t \Phi_\xi + \tilde{\gamma} P(\xi) \Phi_t^2 = -v \int_0^t \int \Phi_t \Gamma(\Phi_\xi, \Phi_t - c_0 \Phi_\xi),$$

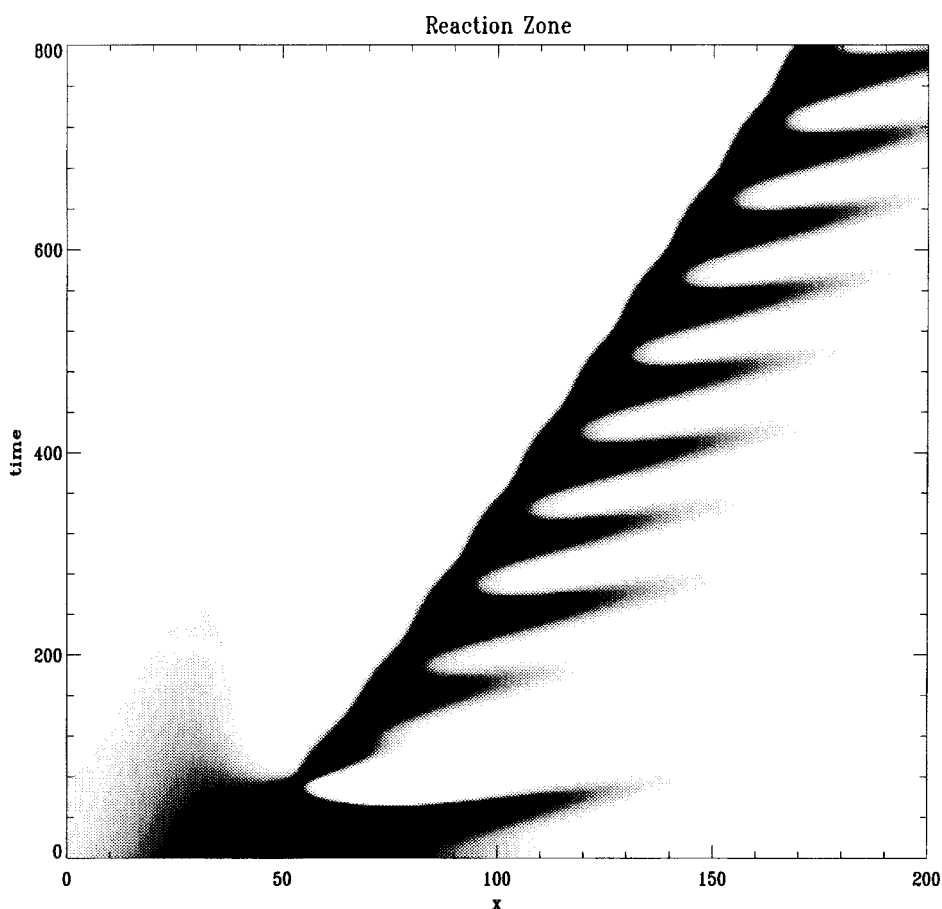


FIG. 7. Space-time density plot of the reaction zone $Z(A, S)$ vs. time, showing persistent oscillations in the three-equation BM. The darker region is where $Z(A, S)$ is above 0.1.

or

$$\begin{aligned} & \frac{1}{2} \|\Phi_t\|_2^2 + \frac{1}{2} (v - c_0)(c_0 - vR_f^{-1}) \|\Phi_\xi\|_2^2 + \int_0^t \int v\tilde{\gamma}Q(\xi)\Phi_t\Phi_\xi + \tilde{\gamma}P(\xi)\Phi_t^2 \\ (7.1) = & \frac{1}{2} \|\Phi_t^{(0)}\|_2^2 + \frac{1}{2} (v - c_0)(c_0 - vR_f^{-1}) \|\Phi_\xi^{(0)}\|_2^2 - v \int_0^t \int \Phi_t \Gamma(\Phi_\xi, \Phi_t - c_0\Phi_\xi). \end{aligned}$$

Multiplying Φ to (4.8), and integrating over (x, t) , we get

$$\begin{aligned} & \int_0^t \int \Phi \Phi_{tt} + (v(1 + R_f^{-1}) - 2c_0)\Phi \Phi_{t\xi} \\ & + \int_0^t \int (c_0 - v)(c_0 - vR_f^{-1})\Phi \Phi_{\xi\xi} + v\tilde{\gamma}Q(\xi)\Phi \Phi_\xi + \tilde{\gamma}P(\xi)\Phi \Phi_t \\ = & - \int_0^t \int v\Phi \Gamma(\Phi_\xi, \Phi_t - c_0\Phi_\xi), \end{aligned}$$

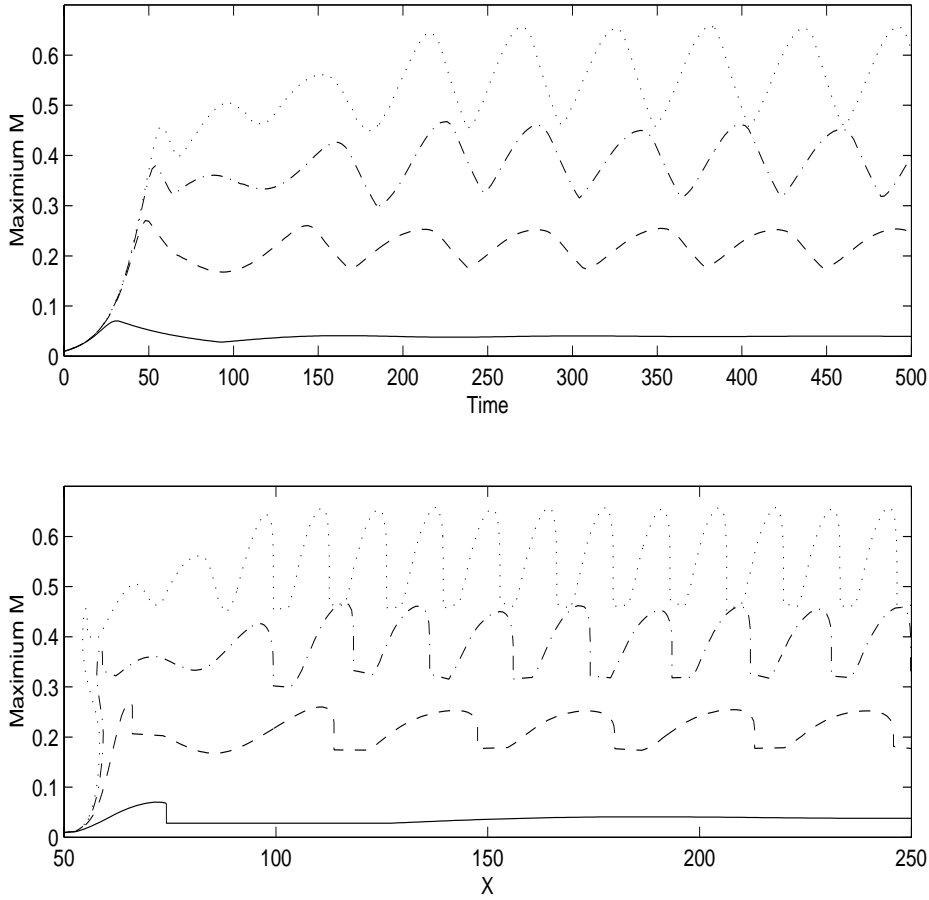


FIG. 8. The plots show the the maximum value of M for the parameter range $R_f = 1.5$ (solid line), 5 (dashed line), 8.5 (dot-dashed), and 12 (dotted line). The frequency of the maximum of M when $b = 0.02$ increases from a steady value when $R_f = 1.5$ to higher and higher oscillatory values as R_f increases. The upper plot shows that the frequency is only weakly dependent on R_f in the time domain. In the lower plot, the fronts slow down at higher R_f and the spatial frequency increases approximately linearly with R_f .

or

$$\begin{aligned}
 & \int_0^t \frac{d}{dt} \int \left[\Phi \Phi_t + (v(1 + R_f^{-1}) - 2c_0) \Phi \Phi_\xi + \frac{\tilde{\gamma} P(\xi)}{2} \Phi^2 \right] \\
 & - \int_0^t \int \Phi_t^2 + (v(1 + R_f^{-1}) - 2c_0) \Phi_t \Phi_\xi \\
 & + \int_0^t \int (v - c_0)(c_0 - vR_f^{-1}) \Phi_\xi^2 - \frac{1}{2} v \tilde{\gamma} Q'(\xi) \Phi^2 \\
 & = -v \int_0^t \int \Phi \Gamma(\Phi_\xi, \Phi_t - c_0 \Phi_\xi),
 \end{aligned}$$

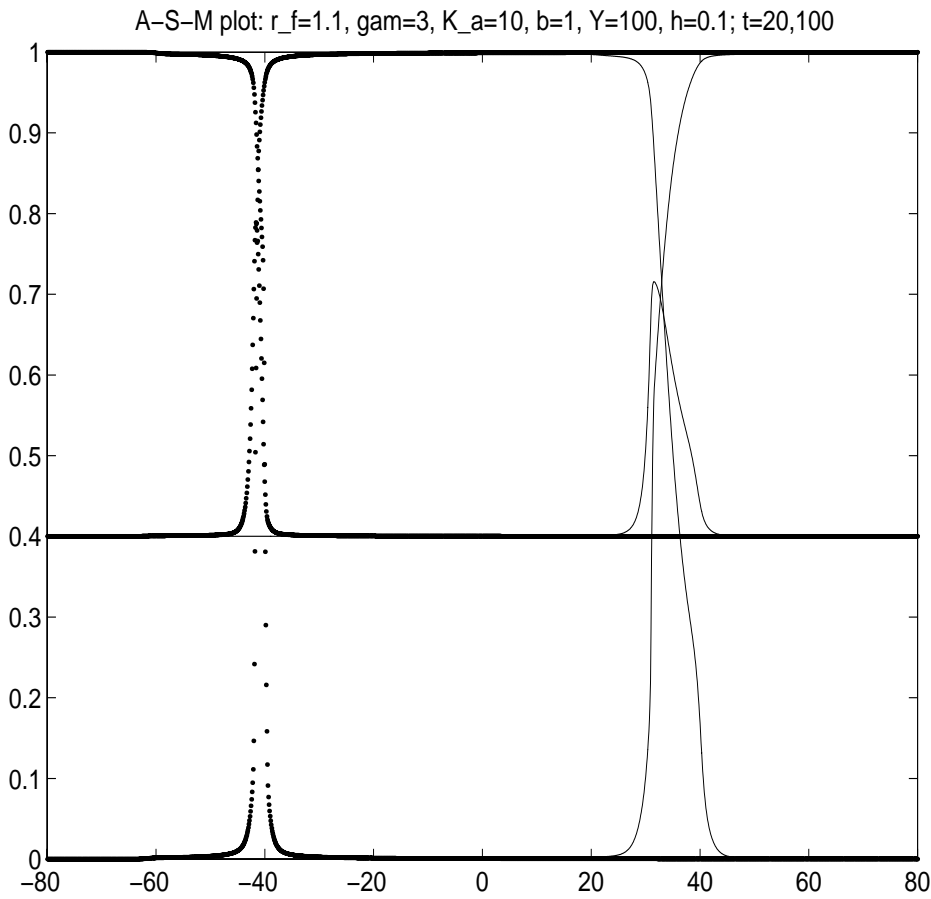


FIG. 9. The profiles of the three components S , A , and M are shown at times $t = 20$ and $t = 100$ for the parameters $Y = 100$, $K_A = K_S = 10$, $b = 0.5$, $\gamma = 3$, and $R_f = 1.1$. The initial $M = M_b = 0.4$ grows and peaks in the overlap region of the the A and S fronts.

or

$$\begin{aligned}
 & \int \left[\Phi \Phi_t + (v(1 + R_f^{-1}) - 2c_0) \Phi \Phi_\xi + \frac{\tilde{\gamma} P(\xi)}{2} \Phi^2 \right] \\
 & - \int_0^t \int \Phi_t^2 + (v(1 + R_f^{-1}) - 2c_0) \Phi_t \Phi_\xi \\
 & + \int_0^t \int (v - c_0)(c_0 - vR_f^{-1}) \Phi_\xi^2 - \frac{1}{2} v \tilde{\gamma} Q'(\xi) \Phi^2 \\
 & = -v \int_0^t \int \Phi \Gamma(\Phi_\xi, \Phi_t - c_0 \Phi_\xi) \\
 (7.2) \quad & + \int \left[\Phi^{(0)} \Phi_t^{(0)} + (v(1 + R_f^{-1}) - 2c_0) \Phi^{(0)} \Phi_\xi^{(0)} + \frac{\tilde{\gamma} P(\xi)}{2} (\Phi^{(0)})^2 \right].
 \end{aligned}$$

Next, let λ be a positive parameter to be chosen. Multiplying (7.2) by λ and

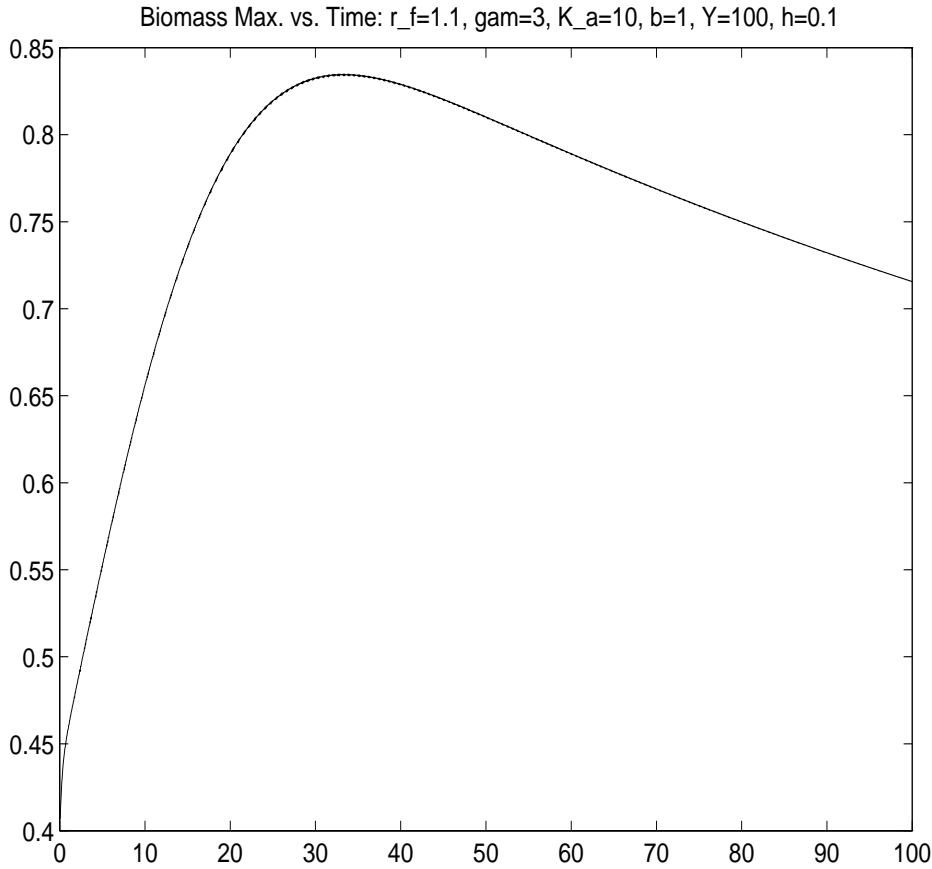


FIG. 10. The spatial maximum of the biomass for the simulation shown in Figure 9 increases until $t = 30$ when it saturates at $M = 0.83$ and then slowly decays.

adding the resulting expression to (7.1) we get

$$\begin{aligned}
 & \int \left[\frac{1}{2} \Phi_t^2 + \frac{1}{2} (v - c_0) (c_0 - v R_f^{-1}) \Phi_\xi^2 + \lambda \Phi \Phi_t \right. \\
 & \quad \left. + \lambda (v (1 + R_f^{-1}) - 2c_0) \Phi \Phi_\xi + \frac{\lambda \tilde{\gamma}}{2} P(\xi) \Phi^2 \right] \\
 & + \int_0^t \int [\tilde{\gamma} P(\xi) \Phi_t^2 + v \tilde{\gamma} Q(\xi) \Phi_t \Phi_\xi + \lambda (v - c_0) (c_0 - v R_f^{-1}) \Phi_\xi^2 \\
 & \quad - \lambda \Phi_t^2 - \lambda (v (1 + R_f^{-1}) - 2c_0) \Phi_t \Phi_\xi] - \frac{\lambda v \tilde{\gamma}}{2} \int_0^t \int Q'(\xi) \Phi^2 \\
 & = -v \int_0^t \int (\Phi_t + \lambda \Phi) \Gamma(\Phi_\xi, \Phi_t - c_0 \Phi_\xi) \\
 (7.3) \quad & + c_0 \|(\Phi^{(0)}, \Phi_t^{(0)}, \Phi_\xi^{(0)})\|_2^2.
 \end{aligned}$$

We select λ such that

$$(7.4) \quad \frac{1}{4} \Phi_t^2 + \lambda \Phi \Phi_t + \frac{\lambda \tilde{\gamma}}{8} P(\xi) \Phi^2 \geq 0,$$

$$(7.5) \quad \frac{1}{4}(v - c_0)(c_0 - vR_f^{-1})\Phi_\xi^2 + \lambda(v(1 + R_f^{-1}) - 2c_0)\Phi\Phi_\xi + \frac{\lambda\tilde{\gamma}}{8}P(\xi)\Phi^2 \geq 0,$$

$$(7.6) \quad \frac{1}{8}\tilde{\gamma}P(\xi) \geq \frac{\tilde{\gamma} \min P(\xi)}{8} \equiv \frac{\tilde{\gamma}P}{8} \geq \lambda,$$

and

$$(7.7) \quad \begin{aligned} & \frac{1}{2}(\tilde{\gamma}P(\xi) - \lambda)\Phi_t^2 + [v\tilde{\gamma}Q(\xi) - \lambda(v(1 + R_f^{-1}) - 2c_0)]\Phi_t\Phi_\xi \\ & + \frac{1}{2}\lambda(v - c_0)(c_0 - vR_f^{-1})\Phi_\xi^2 \geq 0. \end{aligned}$$

Under (7.4)–(7.7) we have from (7.3)

$$(7.8) \quad \begin{aligned} & \frac{1}{4}\|\Phi_t\|_2^2 + \frac{1}{4}\lambda\tilde{\gamma}P\|\Phi\|_2^2 + \frac{1}{4}(v - c_0)(c_0 - vR_f^{-1})\|\Phi_\xi\|_2^2 \\ & - \frac{1}{2}\lambda v\tilde{\gamma} \int_0^t \int Q'(\xi)\Phi^2 + \int_0^t \int \frac{7}{16}\tilde{\gamma}P\Phi_t^2 + \frac{\lambda}{2}(v - c_0) \left(c_0 - \frac{v}{R_f}\right)\Phi_\xi^2 \\ & \leq -v \int_0^t \int (\Phi_t + \lambda\Phi)\Gamma(\Phi_\xi, \Phi_t - c_0\Phi_\xi) + c_0\|(\Phi^{(0)}, \Phi_t^{(0)}, \Phi_\xi^{(0)})\|_2. \end{aligned}$$

To ensure (7.4)–(7.7), it is sufficient to impose

$$(7.9) \quad \lambda^2 \leq \frac{1}{8}\lambda\tilde{\gamma}P(\xi),$$

$$(7.10) \quad \lambda(v(1 + R_f^{-1}) - 2c_0)^2 \leq (v - c_0)(c_0 - vR_f^{-1})\frac{1}{8}\tilde{\gamma}P(\xi),$$

$$(7.11) \quad [v\tilde{\gamma}Q(\xi) - \lambda(v(1 + R_f^{-1}) - 2c_0)]^2 \leq \lambda(v - c_0)(c_0 - vR_f^{-1})(\tilde{\gamma}P(\xi) - \lambda).$$

It is easy to satisfy (7.9) and (7.10) by choosing λ such that

$$(7.12) \quad \lambda \leq \min \left[\frac{\tilde{\gamma}P}{8}, (v - c_0)(c_0 - vR_f^{-1}) \left(\frac{\tilde{\gamma}P}{8} \right) (v(1 + R_f^{-1}) - 2c_0)^{-2} \right].$$

For (7.11) we write

$$(7.13) \quad \begin{aligned} Q &= (R_f - 1)A_0(1 - c_0v^{-1}) + \gamma(R_f - 1)S_0 \left(1 - \frac{c_0R_f}{v} \right) \\ &= (R_f - 1)^2A_0 \frac{\gamma S_+}{\gamma R_f S_+ + A_-} - \gamma(R_f - 1)^2S_0 \frac{A_-}{\gamma R_f S_+ + A_-} \\ &= (R_f - 1)^2\gamma(A_0S_+ - S_0A_-)(\gamma R_f S_+ + A_-)^{-1} \end{aligned}$$

and

$$(7.14) \quad P = (R_f - 1)(A_0 + R_f\gamma S_0).$$

Also

$$(7.15) \quad (v(1 + R_f^{-1}) - 2c_0) = v(R_f - 1) \frac{\gamma S_+ - R_f^{-1}A_-}{\gamma R_f S_+ + A_-}$$

and

$$(7.16) \quad (v - c_0) \left(c_0 - \frac{v}{R_f} \right) = \frac{v^2}{R_f} \frac{\gamma S_+ A_- (R_f - 1)}{(\gamma R_f S_+ + A_-)^2}.$$

Thus, (7.11) becomes

$$(7.17) \quad \begin{aligned} & \left(\tilde{\gamma} \gamma (R_f - 1)^2 (A_0 S_+ - S_0 A_-) - \lambda (R_f - 1) (\gamma S_+ - R_f^{-1} A_-) \right)^2 \\ & \leq \lambda \gamma S_+ A_- (1 - R_f^{-1}) (\tilde{\gamma} (R_f - 1) (A_0 + R_f \gamma S_0) - \lambda). \end{aligned}$$

Setting $\lambda = \tilde{\gamma} \mu$, we see that $\tilde{\gamma}$ scales out of (7.12) and (7.17), and we need only to satisfy

$$(7.18) \quad \mu \leq \frac{P}{8} \min[1, (v - c_0)(c_0 - v R_f^{-1})(v(1 + R_f^{-1}) - 2c_0)^{-2}]$$

and

$$(7.19) \quad \begin{aligned} & \left(\gamma (R_f - 1)^2 (A_0 S_+ - S_0 A_-) - \mu (R_f - 1) (\gamma S_+ - R_f^{-1} A_-) \right)^2 \\ & \leq \mu \gamma S_+ A_- (1 - R_f^{-1}) ((R_f - 1)(A_0 + R_f \gamma S_0) - \mu). \end{aligned}$$

Using (7.15) and (7.16), we write (7.18) and (7.6) as

$$(7.20) \quad \mu \leq \frac{P}{8} \min[1, R_f^{-1} (\gamma S_+ - R_f^{-1} A_-)^{-2} (R_f - 1)^{-1} \gamma S_+ A_-],$$

$$(7.21) \quad \begin{aligned} & \left(\gamma (R_f - 1)^2 (A_0 S_+ - S_0 A_-) - \mu (R_f - 1) (\gamma S_+ - R_f^{-1} A_-) \right)^2 \\ & \leq \mu \gamma S_+ A_- (1 - R_f^{-1}) (P - \mu). \end{aligned}$$

To analyze (7.20) and (7.21), let us estimate \underline{P} . Recalling (3.4), we get

$$(7.22) \quad \begin{aligned} P &= (u_0 - R_f w_0) + R_f (u_0 - w_0) \\ &= \left((1 + R_f) \frac{v}{c_0} - 2R_f \right) w_0 + (1 + R_f) \left(\frac{v}{c_0} - 1 \right) A_- \\ &= (R_f - 1) (\gamma S_+ + A_-)^{-1} [(\gamma R_f S_+ - A_-) w_0 \\ & \quad + (1 + R_f) \gamma S_+ A_-]. \end{aligned}$$

We find that $-A_- \leq w_0 \leq \gamma S_+$; therefore, if $\gamma R_f S_+ \geq A_-$, we have

$$(7.23) \quad \begin{aligned} P &\geq (R_f - 1) (\gamma S_+ + A_-)^{-1} [(\gamma R_f S_+ - A_-)(-A_-) + (1 + R_f) \gamma S_+ A_-] \\ &= \frac{R_f - 1}{\gamma S_+ + A_-} (A_-^2 + \gamma S_+ A_-) = (R_f - 1) A_-, \end{aligned}$$

whereas if $\gamma R_f S_+ < A_-$, we have

$$(7.24) \quad \begin{aligned} P &\geq (R_f - 1) (\gamma S_+ + A_-)^{-1} [(\gamma R_f S_+ - A_-) \gamma S_+ + (1 + R_f) \gamma S_+ A_-] \\ &= \gamma R_f S_+ (R_f - 1). \end{aligned}$$

It follows that

$$(7.25) \quad P \geq \underline{P} \equiv (R_f - 1) \min[\gamma R_f S_+, A_-].$$

Therefore, (7.20) is simply

$$(7.26) \quad \mu \leq \frac{1}{8} \min[\gamma R_f S_+, A_-] \min[(R_f - 1), R_f^{-1}(\gamma S_+ - R_f^{-1} A_-)^{-2} \gamma S_+ A_-].$$

To ensure (7.21), it is sufficient to have

$$(7.27) \quad 2\mu(R_f - 1)^2(\gamma S_+ - R_f^{-1} A_-)^2 \leq \frac{\gamma S_+ A_-}{2R_f} (R_f - 1)(\underline{P} - \mu),$$

$$(7.28) \quad 2\gamma^2(R_f - 1)^4(A_0 S_+ - S_0 A_-)^2 \leq \frac{\gamma \mu S_+ A_-}{2R_f} (R_f - 1)(\underline{P} - \mu).$$

Because of (7.20), (7.27) holds if

$$2\mu(R_f - 1)(\gamma S_+ - R_f^{-1} A_-)^2 \leq \frac{7\gamma S_+ A_- \underline{P}}{16R_f},$$

or if

$$(7.29) \quad \begin{aligned} \mu &\leq \frac{7\gamma S_+ A_- \underline{P}}{32R_f(R_f - 1)(\gamma S_+ - R_f^{-1} A_-)^2} \\ &= \frac{7\gamma S_+ A_-}{32R_f(\gamma S_+ - R_f^{-1} A_-)^2} \min[\gamma R_f S_+, A^-]. \end{aligned}$$

Similarly, for (7.28) it is enough to have

$$2\gamma^2(R_f - 1)^4(A_0 S_+ - S_0 A_-)^2 \leq \frac{7\mu\gamma S_+ A_- (R_f - 1)\underline{P}}{16R_f},$$

or

$$2\gamma^2(R_f - 1)^2(A_0 S_+ - S_0 A_-)^2 \leq \frac{7\mu\gamma S_+ A_-}{16R_f} \min[\gamma R_f S_+, A_-],$$

which is true if we require

$$2\gamma^2(R_f - 1)^2(A_- S_+)^2 \leq \frac{7\mu\gamma S_+ A_-}{16R_f} \min[\gamma R_f S_+, A_-],$$

or

$$(7.30) \quad (R_f - 1)^2 \leq \frac{7\mu}{32\gamma R_f A_- S_+} \min[\gamma R_f S_+, A_-].$$

Now it follows from (7.26), (7.29), and (7.30) that

$$\begin{aligned} \frac{32}{7}(R_f - 1)^2 \frac{\gamma R_f A_- S_+}{\min[\gamma R_f S_+, A_-]} &\leq \mu \leq \frac{1}{8} \min[\gamma R_f S_+, A_-] \\ &\times \min[(R_f - 1), R_f^{-1}(\gamma S_+ - R_f^{-1} A_-)^{-2} \gamma S_+ A_-], \end{aligned}$$

which is true for a positive number μ if

$$(7.31) \quad \begin{aligned} \frac{32}{7}(R_f - 1)^2 \gamma R_f A_- S_+ &\leq \frac{1}{8} (\min[\gamma R_f S_+, A_-])^2 \\ &\times \min[(R_f - 1), R_f^{-1}(\gamma S_+ - R_f^{-1} A_-)^{-2} \gamma S_+ A_-]. \end{aligned}$$

Under condition (7.31), we continue to estimate higher derivatives. Differentiating (4.8) to ξ gives

$$\begin{aligned}
 & (\partial_t - c_0 \partial_\xi)^2 \Phi_\xi + v(1 + R_f^{-1})(\partial_t - c_0 \partial_\xi)(\Phi_\xi)_\xi \\
 & + v^2 R_f^{-1}(\Phi_\xi)_{\xi, \xi} + v \tilde{\gamma} Q(\xi)(\Phi_\xi)_\xi + \tilde{\gamma} P(\xi)(\Phi_\xi)_t \\
 (7.32) \quad & = -v \tilde{\gamma} Q_\xi \Phi_\xi - \tilde{\gamma} P_\xi \Phi_t - v \Gamma_\xi \equiv -v \tilde{\Gamma}.
 \end{aligned}$$

Multiplying $(\Phi_\xi)_t$ to (7.32) and integrating over (x, t) , we find

$$\begin{aligned}
 & \frac{1}{2} \|(\Phi_\xi)_t\|_2^2 + \frac{1}{2}(v - c_0)(c_0 - v R_f^{-1}) \|(\Phi_\xi)_\xi\|_2^2 \\
 & + \int_0^t \int v \tilde{\gamma} Q(\xi)(\Phi_\xi)_t (\Phi_\xi)_\xi + \tilde{\gamma} P(\xi)(\Phi_\xi)_t^2 \\
 (7.33) \quad & = \frac{1}{2} \|\Phi_{\xi, t}^{(0)}\|_2^2 + \frac{1}{2}(v - c_0)(c_0 - v R_f^{-1}) \|\Phi_{\xi, \xi}^{(0)}\|_2^2 - v \int_0^t \int (\Phi_\xi)_t \tilde{\Gamma},
 \end{aligned}$$

which is analogous to (7.1). Similarly, multiplying (7.32) by Φ_ξ , we find an identity like (7.2). Multiplying the latter identity by a positive parameter λ and adding the resulting equation to (7.33) yields

$$\begin{aligned}
 & \frac{1}{4} \|\Phi_{\xi, t}\|_2^2 + \frac{\lambda \tilde{\gamma}}{4} P \|\Phi_\xi\|_2^2 + \frac{1}{4}(v - c_0)(c_0 - v R_f^{-1}) \|\Phi_{\xi \xi}\|_2^2 \\
 & + \int_0^t \int \frac{1}{2} (\tilde{\gamma} P - \lambda) \Phi_{\xi, t}^2 + \frac{\lambda}{2}(v - c_0)(c_0 - v R_f^{-1}) \Phi_{\xi, \xi}^2 \\
 & + \frac{\lambda v \tilde{\gamma}}{2} \int_0^t \int (-Q'(\xi)) \Phi_\xi^2 \\
 & \leq - \int_0^t \int (\Phi_{\xi, t} + \lambda \Phi_\xi)(v \Gamma_\xi(\Phi_\xi, \Phi_t - c_0 \Phi_\xi) + v \tilde{\gamma} Q' \Phi_\xi + \tilde{\gamma} P' \Phi_t) \\
 & + c_0 \|(\Phi_\xi^{(0)}, \Phi_{t\xi}^{(0)}, \Phi_{\xi\xi}^{(0)})\|_2^2 \\
 & = - \frac{v \tilde{\gamma}}{2} \int Q' \Phi_\xi^2|_0^t - \int_0^t \int \frac{\tilde{\gamma} P''}{2} \Phi_t^2 \\
 & - \lambda v \tilde{\gamma} \int_0^t \int Q' \Phi_\xi^2 - \lambda \tilde{\gamma} \int_0^t \int P' \Phi_t \Phi_\xi + c_0 \|(\Phi_\xi^{(0)}, \Phi_{t\xi}^{(0)}, \Phi_{\xi\xi}^{(0)})\|_2^2 \\
 (7.34) \quad & - \int_0^t \int (\Phi_{\xi, t} + \lambda \Phi_\xi) v \Gamma_\xi(\Phi_\xi, \Phi_t - c_0 \Phi_\xi).
 \end{aligned}$$

Let us now define $N(t) = \sup_{\tau \in [0, t]} \max[\|\Phi\|_{H^2}(\tau), \|\Phi_t\|_{H^1}]$. There is a positive number λ_1 , depending on $v, \tilde{\gamma}, \|(Q', P', P'')\|_\infty$, and λ , such that (7.34) plus (7.8) times λ_1 gives

$$\begin{aligned}
 & N^2(t) + \int_0^t \|(\Phi_t, \Phi_\xi)\|_{H^1}^2(\tau) d\tau \\
 (7.35) \quad & \leq C'_0 \|(\Phi_\xi^{(0)}, \Phi_{t\xi}^{(0)}, \Phi_{\xi\xi}^{(0)})\|_2^2 + C''_0 \int_0^t N(\tau) \|(\Phi_t, \Phi_\xi)\|_{H^1}^2(\tau) d\tau,
 \end{aligned}$$

where $C'_0, C''_0 > 0$, depending only on $v, \tilde{\gamma}, \|(Q', P', P'')\|_\infty, \lambda, c_0$, and R_f . It follows from (7.35) that

$$(7.36) \quad N^2(t) + (1 - C''_0 N(t)) \int_0^t \|(\Phi_t, \Phi_\xi)\|_{H^1}^2(\tau) d\tau \leq C'_0 (\|\Phi^{(0)}\|_{H^2} + \|\Phi_t^{(0)}\|_{H^1})^2.$$

If the initial perturbation is so small that

$$N(0) \leq \sqrt{C_0'}(\|\Phi^{(0)}\|_{H^2} + \|\Phi_t^{(0)}\|_{H^1}) < \frac{1}{2C_0''},$$

then (7.36) implies that $N(t) \leq \frac{1}{2C_0''}$ for all time. Also, $\|(\Phi_t, \Phi_\xi)\|_{H^1} \rightarrow 0$ as $t \rightarrow +\infty$. It follows that

$$\lim_{t \rightarrow +\infty} \sup_{\xi \in \mathbb{R}^1} |U(\xi, t)| = 0, \quad \lim_{t \rightarrow +\infty} \sup_{\xi \in \mathbb{R}^1} |W(\xi, t)| = 0.$$

The asymptotic stability holds under the condition (7.31) or (4.1). The proof is complete.

8. Summary of results. We have shown that the three-component advection-reaction bioremediation system (1.1)–(1.3) in the inviscid limit ($D = 0$) admits unique smooth traveling waves, which are stable under the explicit relaxation condition (2.17). Also under this condition, the three-component system in the hyperbolic scaling limit converges strongly in space and time to a scalar conservation law with piecewise linear flux. When this condition is violated, the traveling fronts oscillate in time and the three-component system does not relax in the sense of strong convergence to a scalar law. We performed both asymptotic analysis and numerical experiments to substantiate the above findings, also an energy stability analysis on the traveling fronts of a reduced two-component model in the relaxation regime.

Acknowledgments. J. Xin would like to thank S. Jin and Z-P. Xin for interesting discussions on relaxation and M. Hays and A. Rado for tips on local numerical softwares. Both authors wish to thank S. Oya and A. Valocchi for helpful communications on the model and their recent works. In addition, we thank D. Holm and B. Travis for organizing the SIAM Workshop on Bioremediation at Los Alamos National Laboratory (June, 1997), where many mathematical and practical issues on bioremediation were addressed.

REFERENCES

- [1] R. C. BORDEN AND P. B. BEDIANT, *Transport of dissolved hydrocarbons influenced by oxygen-limited biodegradation, 1, Theoretical development*, Water Res. Research, 22 (1986), pp. 1973–1982.
- [2] R. C. BORDEN, P. B. BEDIANT, M. D. LEE, C. H. WARD, AND J. T. WILSON, *Transport of dissolved hydrocarbons influenced by oxygen-limited biodegradation, 2, Field application*, Water Res. Research, 22 (1986), pp. 1983–1990.
- [3] R. E. CAFLISCH, *Navier–Stokes and Boltzmann shock profiles for a model gas dynamics*, Comm. Pure. Appl. Math, 32 (1979), pp. 521–554.
- [4] R. CAFLISCH AND G. PAPANICOLAOU, *The fluid dynamical limit of nonlinear model Boltzmann equations*, Comm. Pure. Appl. Math, 32 (1979), pp. 589–616.
- [5] G-Q. CHEN, C. D. LEVERMORE, AND T. P. LIU, *Hyperbolic conservation laws with stiff relaxation terms and entropy*, Comm. Pure. Appl. Math, 47 (1993), pp. 787–830.
- [6] C. CHIANG, C. DAWSON, AND M. WHEELER, *Modeling of in-situ bioremediation of organic compounds in groundwater*, Transport in Porous Media, 6 (1991), pp. 667–702.
- [7] T. R. GINN, C. S. SIMMONS, AND B. D. WOOD, *Stochastic-convective transport with nonlinear reaction: Biodegradation with microbial growth*, Water Res. Research, 31 (1995), pp. 2689–2700.
- [8] A. HESS, P. HOHENER, D. HUNKELER, AND J. ZEYER, *Bioremediation of a diesel fuel contaminated aquifer: Simulation studies in laboratory aquifer columns*, J. Contam. Hydrology, 23 (1996), pp. 329–345.
- [9] S. JIN AND M. KATSOLAKIS, *Relaxation approximation to front propagation*, J. Differential Equations, 138 (1997), pp. 380–387.

- [10] S. KAWASHIMA AND A. MATSUMURA, *Asymptotic stability of traveling wave solutions of a system of one-dimensional gas motion*, Comm. Math. Phys., 101 (1985), pp. 97–127.
- [11] P. D. LAX, *Hyperbolic Systems of Conservation Laws and the Mathematical Theory of Shock Waves*, CBMS-NSF Regional Conf. Ser. in Appl. Math. 11, SIAM, Philadelphia, 1973.
- [12] R. LEVEQUE, *Numerical Methods for Conservation Laws*, Birkhäuser-Verlag, Basel, Switzerland, 1992.
- [13] K. MACQUARRIE AND E. SUDICKY, *Simulation of biodegradable organic contaminants in groundwater*, Water Res. Research, 22 (1990), pp. 1207–1216.
- [14] F. J. MOLZ, M. A. WIDDOWSON, AND L. D. BENEFIELD, *Simulation of microbial growth dynamics coupled to nutrient and oxygen transport in porous media*, Water Res. Research, 22 (1986), pp. 1207–1216.
- [15] R. MURRAY, *Traveling Waves, Relaxation and Oscillation in a Model for Bioremediation*, Ph.D. dissertation, Program in Applied Math, University of Arizona, Tucson, 1999.
- [16] R. MURRAY AND J. XIN, *Existence of traveling waves in a biodegradation model for organic contaminants*, SIAM J. Math. Anal., 30 (1999), pp. 72–94.
- [17] NATIONAL RESEARCH COUNCIL, *In Situ Bioremediation, When Does it Work?*, Water Science and Technology Board, National Academy Press, Washington D.C., 1993.
- [18] J. ODENCRANTZ, A. VALOCCHI, AND B. RITTMANN, *Modeling the interaction of sorption and biodegradation on transport in groundwater in situ bioremediation systems*, in Proceedings of the 1993 Groundwater Modeling Conference, E. Poeter et al., eds., Golden, CO, 1993.
- [19] S. OYA AND A. VALOCCHI, *Characterization of traveling waves and analytical estimation of pollutant removal in one-dimensional subsurface bioremediation modeling*, Water Res. Research, 33 (1997), pp. 1117–1127.
- [20] S. OYA AND A. VALOCCHI, *Analytical approximation of biodegradation rate for an in situ bioremediation of groundwater under ideal radial flow conditions*, J. Contam. Hydrology, 31 (1998), pp. 275–293.
- [21] G. B. WHITHAM, *Linear and Nonlinear Waves*, Wiley, New York, 1974.
- [22] J. XIN, *Fluid Limit and Free Boundaries in Biodegradation*, in Free Boundary Problems: Theory and Applications, N. Kenmochi, ed., GAKUTO Internat. Ser. Math. Sci. Appl. 13, Gakkōtoshō, Tokyo, pp. 429–440.
- [23] J. XIN AND D. ZHANG, *Statistical analysis of biodegradation fronts in one-dimensional heterogeneous porous media*, Advances in Water Resources, 22 (1998), pp. 103–116.
- [24] Z-P. XIN, *The fluid dynamic limit of the Broadwell model of the nonlinear Boltzmann equations in the presence of shocks*, Comm. Pure Appl. Math, 44 (1991), pp. 679–713.